# Entanglement Dynamics in Monitored Systems and the Role of Quantum Jumps

Youenn Le Gal,[1] Xhek Turkeshi,[1,2] and Marco Schirò[1,*]

[1] *Jeunes Equipes de l'Institut de Physique du Collège de France (JEIP), UAR 3573 CNRS, Collège de France, Paris Sciences et Lettres (PSL) Research University, 11, place Marcelin Berthelot, Paris Cedex 05 75231, France*

[2] *Institut für Theoretische Physik, Universität zu Köln, Zülpicher Strasse 77, Köln 50937 Germany*

(Received 14 January 2024; accepted 26 June 2024; published 8 August 2024)

Monitored quantum many-body systems display a rich pattern of entanglement dynamics, which is unique to this nonunitary setting. This work studies the effect of quantum jumps on the entanglement dynamics beyond the no-click limit corresponding to a deterministic non-Hermitian evolution. To this aim, we introduce a new tool that looks at the statistics of entanglement-entropy gain and loss after and in between quantum jumps. This insight allows us to build a simple stochastic model of a random walk with partial resetting, which reproduces the entanglement dynamics, and to dissect the mutual role of jumps and non-Hermitian evolution on the entanglement scaling. We apply these ideas to the study of measurement-induced transitions in monitored fermions. We demonstrate that significant deviations from the no-click limit arise whenever quantum jumps strongly renormalize the non-Hermitian dynamics, as in the case of models with $U(1)$ symmetry at weak monitoring. On the other hand, we show that the weak-monitoring phase of the Ising chain leads to a robust subvolume logarithmic phase due to weakly renormalized non-Hermitian dynamics.

DOI: 10.1103/PRXQuantum.5.030329

## I. INTRODUCTION

The spreading of quantum entanglement under unitary dynamics displays remarkable robustness and universality [1–3]. For example, in clean systems with short-ranged interactions, the entanglement entropy is generally expected to grow linearly in time and to saturate to a volume law [4,5]; the violation of this behavior is often taken as a smoking gun of nonergodic dynamics [6]. On the other hand, nonunitary processes such as quantum measurements can strongly affect how entanglement spreads throughout the system. Out of this competition, a novel type of measurement-induced phase transition (MIPT) in the entanglement content of the system has been discovered [7–9].

Entanglement transitions due to measurements have been studied broadly in two somewhat different settings; on the one hand, in the stochastic dynamics encoded in a quantum many-body trajectory describing the evolution of the system conditioned to a set of measurement outcomes. In this setting, the criticality is hidden in the rare fluctuations of the measurement process, probed by a nonlinear functional of the state such as the entanglement entropy or the purity in a dynamical purification protocol [10], while conventional observables averaged over the noise are usually transparent to it. This makes the theoretical description and experimental detection of MIPT particularly challenging, even though recent progress has been made [11–13]. On the theoretical front, volume-to-area law entanglement transitions have been reported in monitored random circuits [14–23] and nonintegrable Hamiltonians [24–28] with projective or weak measurements. Monitored noninteracting systems, on the other hand, are not expected to sustain a volume-law phase [29,30]. Still, a critical subvolume phase, the origin and stability of which are currently under debate [31–37], has been numerically found in several works [38–48].

A different limit of the measurement problem is obtained by postselecting atypical trajectories corresponding to specific measurement outcomes. To fix the ideas, consider, e.g., the quantum jump (QJ) dynamics corresponding to a photocounting monitoring protocol [49–51]: here, abrupt random quantum jumps (clicks) intersperse the deterministic evolution driven by a non-Hermitian Hamiltonian, which accounts for the measurement back action. Postselecting on the trajectory where no click has happened corresponds to purely non-Hermitian dynamics. In this limit, several works have reported measurement-induced

*Contact author: marco.schiro@college-de-france.fr

entanglement transitions and highlighted their relation with the spectral properties of the non-Hermitian Hamiltonian [52–63].

The relation between these two limits of the measurement problem, particularly concerning the entanglement dynamics, is not well understood. Is the no-click dynamics stable enough to the inclusion of QJs, which should be seen as irrelevant perturbations? Or, on the contrary, do QJs completely change the entanglement structure of the monitored system? These questions ultimately go beyond measurement-induced transitions and touch upon the relevance of non-Hermitian Hamiltonians in the description of open quantum systems [64–70].

To understand the role of QJs and non-Hermitian evolution on the entanglement dynamics in monitored systems, we introduce a new tool: the statistics of the entanglement-entropy changes after and in between QJs. We show that, on average, QJs induce an entanglement-entropy loss while the non-Hermitian evolution causes a gain, although the statistics display rather broad tails and fluctuations. Using the full statistics of entanglement gain and loss, we propose a classical stochastic random-walk (RW) model with partial resetting for the entanglement dynamics, that we show to reproduce the full QJ dynamics. More importantly, the entanglement gain and loss picture clarifies the mutual role of quantum jumps and non-Hermitian evolution in the scaling of entanglement entropy in the steady state, with direct implications for the associated MIPT.

We showcase our new method by studying three models of monitored free fermions: the Ising chain, the monitored Su-Schrieffer-Heeger (SSH) chain, and a model of free fermions with $U(1)$ symmetry. These models are interesting for two reasons: first, they differ in their global symmetry, a fact that is believed to play a critical role in the stability of the MIPT; second, their entanglement transition in the no-click limit has been studied in detail [55,56]. By solving the full stochastic QJ dynamics for these models and computing the entanglement entropy, we show that QJs have remarkably different impacts on their phase diagrams, as compared to the no-click limit. We understand this difference through a detailed analysis of the entanglement gain and loss, which reveals the crucial role of quantum jumps in *renormalizing* the effective non-Hermitian dynamics with respect to the bare no-click limit. We show that this renormalization, or the lack thereof, can naturally explain the different behaviors of quantum jumps in the three models and provide a criterion for the relevance of the no-click limit. Finally, we demonstrate how the entanglement gain-loss picture and the associated classical model remain valid even in the presence of interactions breaking Gaussianity.

The paper is structured as follows. In Sec. II, we review the background material: we introduce the QJ measurement protocol and the models we will consider throughout this work as well as the quantities we will use to characterize them. In Sec. III, we present the main quantity of interest for this work, namely, the statistics of entanglement gain and loss, that we use to construct a classical stochastic model for the entanglement dynamics. In Sec. IV, we present several applications of this tool to the study of MIPT in models of monitored free fermions. In particular, we use the insights from this model to discuss the role of jumps and non-Hermitian dynamics on the scaling of the entanglement and the MIPT. Finally, Sec. VI contains our conclusions and future perspectives. In the appendixes, we provide further methodological details and results relevant for our work.

## II. BACKGROUND

In this section, we summarize relevant background material, including the quantum jump protocol to continuously monitor a quantum system and its sampling via the Monte Carlo wave-function method and the waiting-time distribution (WTD). We then define the models we focus on throughout the paper and the main quantities we use to characterize their dynamics.

### A. Monitoring by quantum jumps

In this work, we are interested in the dynamics of continuously monitored quantum systems [51]. The setup we have in mind is sketched in Fig. 1, namely, a fermionic chain where each lattice site is coupled to a measurement apparatus that weakly and continuously monitors some local observable of the chain. We are interested in the dynamics of the system wave function conditioned to the measurement outcomes, which realizes a so-called quantum trajectory. Different measurement protocols give rise to different types of stochastic evolutions. Here, we focus on the quantum jump protocol [49,71,72], corresponding to the experimentally relevant photocounting process and which is described by the following stochastic Schrödinger equation:

$$d|\Psi(t)\rangle = -idt\left\{H - \frac{i}{2}\sum_i (L_i^\dagger L_i - \langle L_i^\dagger L_i\rangle_t)\right\}|\Psi(t)\rangle + \sum_i d\xi_i\left\{\frac{L_i}{\sqrt{\langle L_i^\dagger L_i\rangle}} - 1\right\}|\Psi(t)\rangle. \tag{1}$$

where $H$ is the Hamiltonian of the fermionic chain (we will give explicit expression in Sec. II C), $L_i, L_i^\dagger$ are the jump operators defined on each lattice site, which describe the measurement process, and $d\xi_i \in \{0,1\}$ is an increment for the inhomogeneous Poisson process with average $P(d\xi_i = 1) = dt\langle\psi(t)|L_i^\dagger L_i|\psi(t)\rangle$.

The dynamics in Eq. (1) is composed of a deterministic part (for $d\xi_i = 0$) that corresponds to an effective

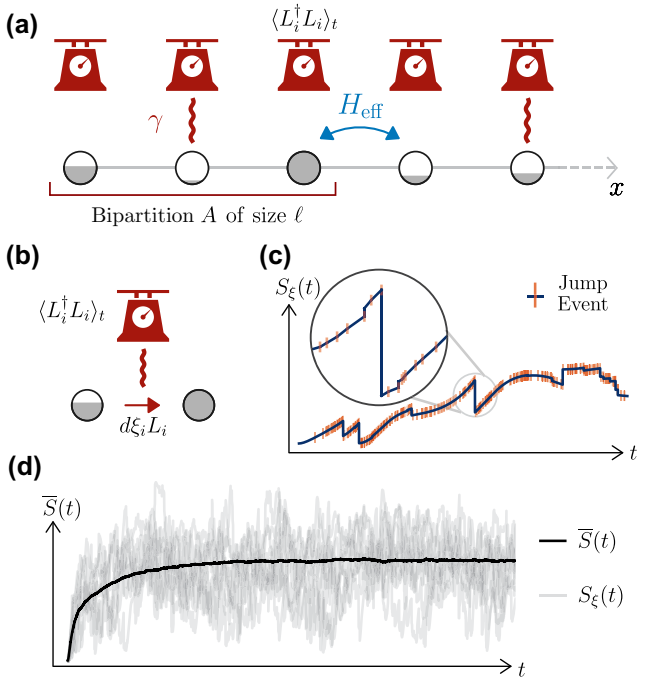


FIG. 1. (a),(b) A sketch of the setup: a monitored fermionic chain (a) evolving under the quantum jump (b) protocol, characterized by a deterministic evolution driven by (a) a non-Hermitian Hamiltonian $H_{\rm eff}$ and (b) stochastic quantum jumps. (c) The quantum trajectory: we are interested in the stochastic dynamics of the wave function and in particular in its entanglement structure, as measured from the bipartite entanglement entropy $S_\xi(t)$ [see (a) for the partition]. (d) Typical quantum trajectory evolutions (ten realizations) for the entanglement entropy and its average over the measurement noise $\xi$.

non-Hermitian Hamiltonian $H_{\rm eff}$ given by

$$H_{\rm eff} = H - \frac{i}{2}\sum_i L_i^\dagger L_i \tag{2}$$

and a stochastic one, the last term in Eq. (1), due to the action of QJs. The effective Hamiltonian $H_{\rm eff}$ is non-Hermitian because of the measurement back action, encoded in the last term of Eq. (2). Its role is to control the dynamics in the so-called *no-click* limit, when no jumps happen during the quantum trajectory, as well as the evolution in between two subsequent quantum jumps. We note that the evolution of the system is state dependent (and thus nonlinear); see the counter-term appearing in Eq. (1), to ensure the normalization.

The QJ evolution in Eq. (1) is solved using Monte Carlo methods [73], either via a first-order integration scheme that introduces an explicit discretization $dt$ to sample the QJs or using higher-order schemes. The former approach has the drawback of not having a natural way to control the accuracy of the simulation, which is instead empirically benchmarked by considering different choices of $dt$ and checking that there is no qualitative difference in the disorder averages. We overcome this limitation considering a higher-order scheme that is based on sampling the time at which subsequent jumps happen [73–75], i.e., using the cumulative WTD, defined as

$$F[\Psi,\tau] = 1 - \langle\Psi|e^{iH_{\rm eff}^\dagger\tau}e^{-iH_{\rm eff}\tau}|\Psi\rangle. \tag{3}$$

Specifically, we proceed by iterating the following loop. (i) Assume a normalized state $|\Psi(t_i)\rangle$ is reached at time $t_i$ (possibly the initial time of the dynamics, in which case $|\Psi(t_i)\rangle$ is the initial state). (ii) Extract a random number $r$ uniformly distributed in $[0,1]$ and find the random waiting time $\tau$ for the next jump by solving the equation $r = 1 - F[\Psi(t),\tau]$. (iii) Within the time interval $[t, t+\tau]$, propagate the deterministic non-Hermitian evolution

$$|\Psi(t+\tau)\rangle = \frac{e^{-iH_{\rm eff}\tau}|\Psi(t)\rangle}{||e^{-iH_{\rm eff}\tau}|\Psi(t)\rangle||}. \tag{4}$$

(iv) At time $t+\tau$, a quantum jump occurs. As before, the output channel is chosen splitting the [0,1] interval into segments of size $\langle\Psi(t+\tau)|L_i^\dagger L_i|\Psi(t+\tau)\rangle$ and checking in which one a uniformly drawn random number falls. The jump is immediate and the postmeasurement state after a jump at site $j$ reads

$$|\Psi(t+\tau^+)\rangle = \frac{L_j|\Psi(t+\tau)\rangle}{\sqrt{\langle\Psi(t+\tau)|L_j^\dagger L_j|\Psi(t+\tau)\rangle}}. \tag{5}$$

In a nutshell, a quantum trajectory is specified as a sequence of non-Hermitian quantum quenches interspersed with discontinuous jumps [see Fig. 1(c)] that set the initial conditions for the forthcoming integration steps.

An advantage of this approach is to directly access the WTD or delay function [73,76,77], which encodes the probability distribution of the times between QJs. Its behavior will be discussed for the specific model of interest later on in the paper.

### B. Average versus conditional dynamics and entanglement entropy

The stochastic Schrödinger equation [Eq. (1)] describes the evolution of the conditional state, also called a quantum trajectory. By averaging the density matrix $\rho_\xi(t) = |\psi_\xi(t)\rangle\langle\psi_\xi(t)|$ over the stochastic noise $\xi$ in Eq. (1), one recovers a Lindblad master equation for the average state (This time-dependent random variable $\xi$ is used to label the different trajectories.) These two descriptions are equivalent with regard to simple observables, which are linear functionals of the conditional state and, indeed, quantum trajectories are also called *unravelings* of the Lindblad master equation [78]. The stochastic dynamics, however,

contain richer information: if one is interested in quantities that are nonlinear in the state and sensitive to higher moments of the density matrix, then averaging over the measurement noise gives rise to physics that is not captured by the Lindblad or average state. A relevant example is provided by the (von Neumann) entanglement entropy, defined as [79,80]

$$S_\xi(t) = -\mathrm{tr}_A\left[\rho_\xi^A(t)\ln\rho_\xi^A(t)\right], \tag{6}$$

where we have introduced a partition $A\cup B$ in the system (cf. Fig. 1) and the reduced density matrix $\rho_\xi^A(t) = \mathrm{tr}_B|\Psi_\xi(t)\rangle\langle\Psi_\xi(t)|$. Therefore, the entanglement entropy will be a fluctuating quantity evolving stochastically (see Fig. 1). In this work, we will be mainly concerned with the average entanglement entropy, given by

$$\overline{S}(t) = \int \mathcal{D}\xi P(\xi) S_\xi(t), \tag{7}$$

where the average is taken over the measurement noise $\xi$. In particular, we will discuss how the steady-state entanglement entropy scales with the size of the subsystem $\ell$. In thermal equilibrium or for unitary dynamics, this is known to sharply characterize the nature of a given phase [80], depending on whether this scaling is proportional to the volume of the subsystem ($S\sim\ell$ in one dimension) or to its area ($S\sim$ const. in one dimension), possibly with logarithmic corrections as for quantum critical states.

### C. Models of monitored fermions

In this work, we consider three models of monitored free fermions with different internal symmetries and measurement operators, leading to different non-Hermitian Hamiltonian. Furthermore, for one of these cases, we also discuss the role of interactions breaking Gaussianity. The first model is the quantum Ising chain in a transverse field,

$$H_{\mathrm{Ising}} = -\sum_{i=1}^{L}\left[J\sigma_i^x\sigma_{i+1}^x + h\sigma_i^z\right], \tag{8}$$

which is mapped via a Jordan-Wigner transformation to

$$H_{\mathrm{Ising}} = -\sum_{i=1}^{L}\left[J(c_i^\dagger c_{i+1} + c_i^\dagger c_{i+1}^\dagger + \mathrm{h.c.}) + h(1-2n_i)\right]. \tag{9}$$

We choose the jump operators

$$L_i = \sqrt{2\gamma}\,n_i, \tag{10}$$

corresponding to monitoring of the local density $n_i = c_i^\dagger c_i$, and obtain the effective non-Hermitian Hamiltonian

$$H_{\mathrm{eff}} = H_{\mathrm{Ising}} - i\gamma\sum_{i=1}^{L} n_i, \tag{11}$$

describing a non-Hermitian Ising model in a complex-valued transverse field [52,55,81]. We contrast the results for the Ising case with models with $U(1)$ symmetry. Specifically, we consider a fermionic SSH chain with two different sublattices $A$ and $B$ and Hamiltonian

$$H_{\mathrm{SSH}} = -\sum_{j=1}^{L}\left[(J-h)c_{A,j}^\dagger c_{B,j-1} + (J+h)c_{A,j}^\dagger c_{B,j} + \mathrm{h.c.}\right]. \tag{12}$$

We choose the jump operators as

$$L_{A,i} = \sqrt{2\gamma}\,n_{A,i} \qquad L_{B,i} = \sqrt{2\gamma}(1-n_{B,i}), \tag{13}$$

namely, we independently and continuously monitor the local density of particles on sublattice $A$, $n_{A,i} = c_{A,i}^\dagger c_{A,i}$, and the local density of holes, $1-n_{B,i} = c_{B,i}c_{B,i}^\dagger$, on sublattice $B$. Using these quantum jump operators, we obtain an effective non-Hermitian Hamiltonian of the form

$$H_{\mathrm{eff}} = H_{\mathrm{SSH}} - i\gamma\sum_{i=1}^{L}(c_{A,i}^\dagger c_{A,i} + c_{B,i}c_{B,i}^\dagger). \tag{14}$$

This non-Hermitian SSH model has been studied in Ref. [56]. Finally, we consider a model of one-dimensional lattice fermions with $U(1)$ symmetry and next-neighbor interactions, described by a Hamiltonian

$$H = -\sum_{j=1}^{L} c_j^\dagger c_{j+1} + \mathrm{h.c.} + V\sum_{i=1}^{L}(1-2n_i)(1-2n_{i+1}) \tag{15}$$

and monitoring of the local density by the jump operators

$$L_i = \sqrt{2\gamma}\,n_i. \tag{16}$$

The associated non-Hermitian Hamiltonian reads

$$H_{\mathrm{eff}} = H - i\gamma\sum_{i=1}^{L} c_i^\dagger c_i. \tag{17}$$

We note that for $V=0$, the model reduces to monitored free fermions that have been extensively studied, while a finite $V$ allows us to discuss the role of many-body interactions breaking Gaussianity. In both cases, we note that the

non-Hermitian Hamiltonian associated with this problem, Eq. (17), is special in the sense that its imaginary part commutes with its real part. As such, the evolution in between quantum jumps is unitary. On the other hand, the first two examples have a nontrivial non-Hermitian evolution and the entanglement transition associated with the no-click limit has been discussed in Ref. [55,56]. The key features of the no-click problem are summarized for completeness in Appendix A.

## III. STATISTICS OF ENTANGLEMENT GAIN AND LOSS

In this section, we introduce the main tool that we will use throughout this work to understand the intertwined role of QJs and non-Hermitian evolution in monitored quantum system: the statistics of entanglement gain and loss. To simplify the presentation, we illustrate our ideas in the context of the monitored Ising chain (defined in Sec. II C), leaving to Sec. IV a detailed application of this tool to MIPT in different models.

Let us consider the stochastic dynamics of the entanglement entropy along a quantum trajectory, plotted in Fig. 2(a): the typical pattern is given by an evolution driven by the non-Hermitian Hamiltonian interrupted abruptly by a discontinuous change in entanglement entropy due to a quantum jump. From this quantum trajectory, we extract three bits of key information. First, the WTD of QJs, $P_{\rm WT}(\tau)$, which represents the probability density of having a waiting time $\tau$ between QJs. As we show in Fig. 2(b), the WTD displays a Poisson behavior, with a rate $K_\gamma^\infty \propto \gamma L$, that gives rise to an average waiting time $\overline{\tau} \sim 1/\gamma L$ (see also Appendix B). Second, we extract the changes to the entanglement entropy at each jump event and in between the jumps (due to the non-Hermitian evolution). As we see from Fig. 2(a), the entanglement entropy can either increase or decrease after a QJ and, similarly, can either grow or diminish during the time between jumps, where non-Hermitian evolution occurs.

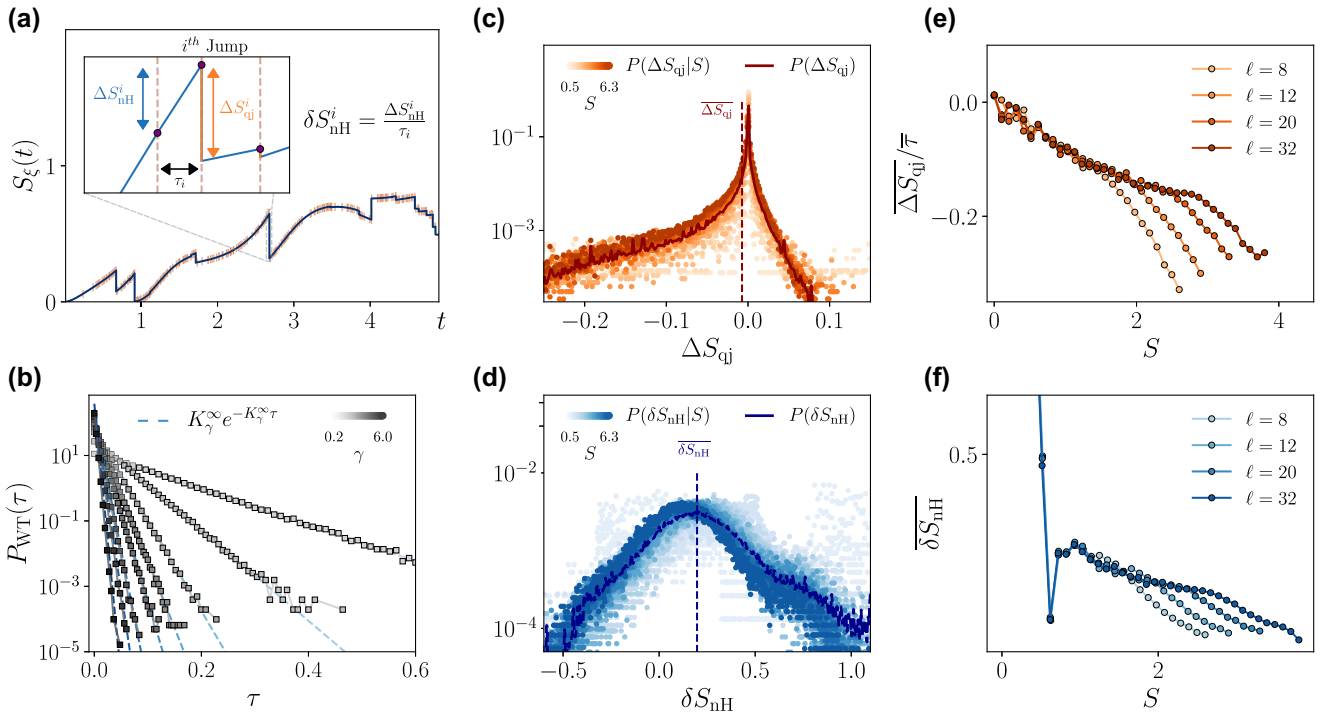


FIG. 2. The statistics of entanglement gain and loss. (a) The evolution of the entanglement entropy along a quantum trajectory, for the monitored Ising chain. The dots symbolize the quantum jumps, while the evolution in between the jumps is due to the non-Hermitian Hamiltonian. From this quantum trajectory, we extract three key quantities (see the inset): (i) the waiting times $\tau_i$ between QJs and the entanglement-entropy change (ii) after a QJ $\Delta S_{\rm qj}$, and (iii) in between QJs $\Delta S_{\rm nH}$. We then construct the corresponding histograms shown in (b)–(d). (b) The waiting-time distribution (WTD) of QJs, $P_{\rm WT}(\tau)$, where $P_{\rm WT}(\tau)d\tau$ is the probability of having an elapsed time between one jump and the next one in the interval $[\tau, \tau + d\tau]$. The Poissonian rate $K_\gamma^\infty$ is the steady-state value of the back action (for more details, see Appendix B). (c) The statistics of entanglement change due to QJs, $P(\Delta S_{\rm qj}|S)$, conditioned on the entanglement content $S$. (d) The corresponding quantity for the non-Hermitian evolution. (e),(f) The average change in the entanglement entropy due to (e) QJs and (f) non-Hermitian evolution. These averages are obtained from the conditional distributions, $P(\Delta S_{\rm qj}|S)$, $P(\Delta S_{\rm nH}|S)$ for system sizes of $L = 128$ and thus are a function of the entanglement entropy $S$ and in these plots we represent the dependence on the subsystem size $\ell$.

Given this pattern, we now ask: what are the statistics of the entanglement-entropy change after a quantum jump and *in between* quantum jumps, i.e., after an evolution step with the non-Hermitian Hamiltonian?

To answer this question, we sample along many quantum trajectories the probability density of observing a change $\Delta S_{\rm qj}$ to the entanglement entropy due to QJs and collect the resulting histogram $P(\Delta S_{\rm qj}|S)$. Similarly, we sample the probability density of observing a change $\delta S_{\rm nH}$ to the entanglement entropy due to the non-Hermitian evolution, which we denote $P(\delta S_{\rm nH}|S)$. Crucially, these are *conditional probabilities* given a certain value of entanglement entropy $S$ before the event. This dependence is a key feature of our approach: the basic idea is to understand whether QJs impact in different ways many-body states that are highly or weakly entangled. In practice, these histograms are obtained by binning stochastic events (jumps or non-Hermitian evolution) according to the *entanglement content* of the state on which they act. To be specific, we say that a state has an entanglement content $S$ at a time $t$ if for $\tau \in [t-\epsilon_t, t+\epsilon_t]$, the entanglement of a state in that time range is such that $|S(|\psi(\tau)\rangle) - S| < \epsilon_S$ (for given $\epsilon_\tau$, $\epsilon_S$).

We plot these histograms in Figs. 2(c) and 2(d) for the monitored Ising chain. The first remarkable observation is that the QJ distribution is strongly peaked around $\Delta S_{\rm qj} = 0$, with broad tails, suggesting that the vast majority of quantum jumps do not substantially change the entanglement entropy. In contrast, rare quantum jumps are responsible for more significant changes and this can also be observed at the level of the trajectory in Fig. 2(a). The asymmetry of the distribution is also interesting to note, since it means that a single QJ is more likely to reduce the entanglement entropy, even though jumps that increase it are also possible. Finally, as we see in Figs. 2(c) and 2(d), the tails of the histogram for the QJs broaden up and acquire a nontrivial $S$ dependence at least for $\Delta S_{\rm qj} < 0$, indicating that highly entangled states are indeed more fragile and prone to be affected by rare QJs. With regard to the entanglement changes during the non-Hermitian evolution in between quantum jumps, we see that the distribution appears centered around a slightly positive value and with a slight asymmetry in the tails, suggesting that the non-Hermitian evolution is primarily responsible for the growth of the entanglement.

In the remainder of this section, we will show how, in fact, the statistics of the entanglement changes, defined above, control the dynamics of the average entanglement entropy and how this can be understood in terms of a simple phenomenological model.

### A. Average entanglement gain and loss

To condense the rich information contained in the full statistics of entanglement changes, we now focus on the first moment of those distributions, corresponding to the average change to the entanglement entropy due to quantum jumps $\overline{\Delta S}_{\rm qj}(S,\ell)$ and to the non-Hermitian evolution $\overline{\delta S}_{\rm nH}(S,\ell)$. The first moments are defined as

$$\overline{\Delta S}_{\rm qj}(S,\ell) \equiv \int_{\Delta S_{\rm qj}} \Delta S_{\rm qj}\, P(\Delta S_{\rm qj}|S) \tag{18}$$

and similarly for $\overline{\delta S}_{\rm nH}(S,\ell)$. We emphasize that these averages [82] depend on the value of the entanglement entropy $S$ and the size of the partition $\ell$, since they are evaluated over the conditional distributions $P(\Delta S_{\rm qj}|S)$ and $P(\delta S_{\rm nH}|S)$, which themselves depend on $\ell$. In Figs. 2(e) and 2(f), we plot these first moments for the monitored Ising chain (at a particular point of the phase diagram) for different subsystem sizes $\ell$. In Fig. 2(f), we see that the change due to non-Hermitian evolution is on average positive, $\overline{\delta S}_{\rm nH} > 0$, i.e., it induces an *entanglement-entropy gain*. This gain is substantial for weakly entangled states, then decreases slowly with the entanglement content. In Fig. 2(e), we plot the change due to QJs, normalized with respect to the average waiting time $\overline{\tau}$. As shown in Appendix C, this ratio remains well defined upon increasing the system size $L$, despite the waiting time vanishing as $\overline{\tau} \sim 1/L$. This is consistent with the idea that a single quantum jump can affect the entanglement entropy of a quantity $O(1/L)$. From Fig. 2(e), we see that $\overline{\delta S}_{\rm qj}/\overline{\tau}$ is negative and decreases with $S$, i.e., QJs on average induce an *entanglement-entropy loss*. They do so the more the state onto which they act is entangled. Interestingly, both averages develop a subsystem-size $\ell$ dependence above a certain threshold entanglement-entropy value. A natural question that we address next is how these average entanglement gains and losses are connected to the entanglement dynamics under QJs and its phase transition.

### B. Classical stochastic model for entanglement dynamics

We now present a classical stochastic model that builds upon the entanglement gain and loss statistics discussed in Sec. III A and gives a physical picture of the entanglement dynamics under QJs. In particular, we model the entanglement evolution as a random walk with random drift and partial resetting [43,83,84], which is sketched in Fig. 3(a) and that we will now describe. We use the previous analysis showing that the waiting time $\tau$ between jumps follows a Poisson law, which means that the random variable can be expressed as $\tau = -\log(r)/K_\gamma^\infty$, where $r \in [0,1]$ is a random number drawn for each jump. Then, during this time $\tau$, we model the change of entanglement due to the non-Hermitian evolution by $\Delta S_{\rm nH} = \tau\ \delta S_{\rm nH}$, where $\delta S_{\rm nH}$ is picked with a probability $P(\delta S_{\rm nH}|S)$ from the previously computed conditional distribution of the

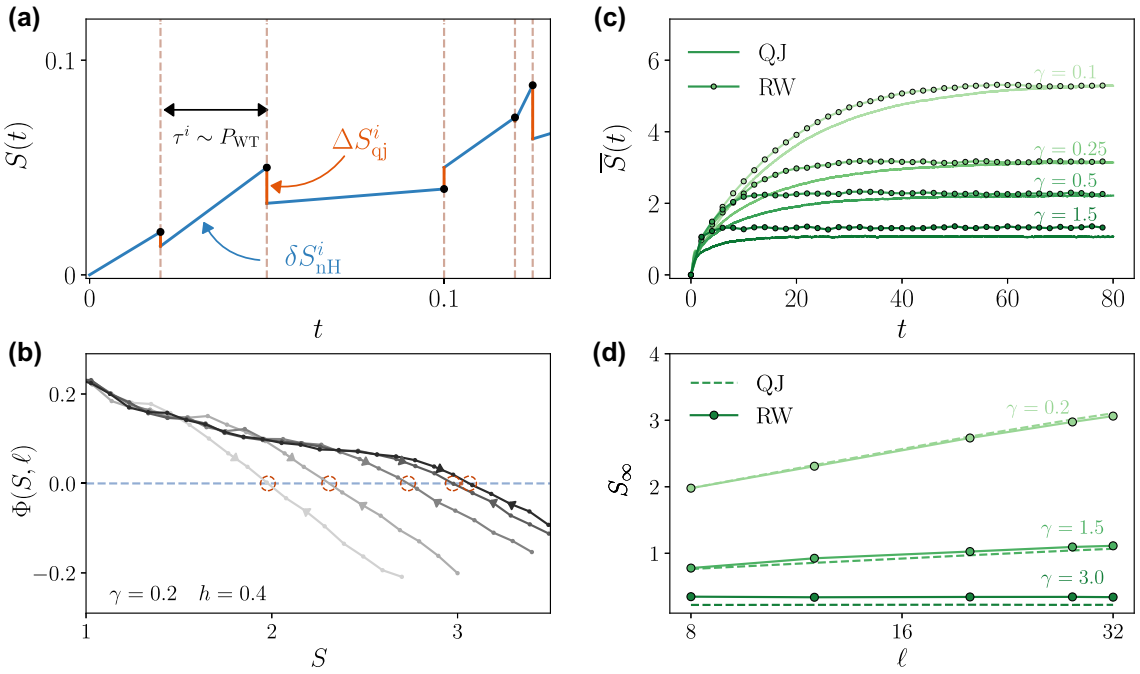


FIG. 3. The stochastic model for the entanglement dynamics. (a) A sketch depicting the entanglement dynamics as a classical random walk (RW) with stochastic drift $\Delta S^i_{\rm nH}$ and resetting $\Delta S^i_{\rm qj}$ drawn from the histograms $P(\Delta S_{\rm nH}|S_i)$ and $P(\Delta S_{\rm qj}|S_i)$ respectively of Fig 2. (b) The total rate of entanglement-entropy growth obtained, for the monitored Ising chain, from the average entanglement gain and loss, according to Eq. (20): $\gamma = 0.2$, $h = 0.4$. We see that the rate $\Phi(S,\ell)$ vanishes at a value $S_\infty(\ell)$ that identifies the steady-state entanglement (circled points). (c) A comparison between the dynamics of the average entanglement entropy obtained from the exact quantum jump dynamics (QJ) and the phenomenological classical RW. (d) A comparison between the steady state $S_\infty$ obtained from the stochastic model and the long-time limit of the entanglement entropy obtained from the full QJ dynamics, showing perfect agreement.

effective non-Hermitian slopes. After time $\tau$, the instantaneous QJ happens and we model the change it has on the entanglement entropy by $\Delta S_{\rm qj}$, which is drawn with a probability $P(\Delta S_{\rm qj}|S)$ from the corresponding probability distribution. In both cases, the entropy $S$ corresponds to the entanglement before the event (i.e., before the jump or before the non-Hermitian evolution). The probability distributions that we use here are taken from the exact sampling of quantum trajectories, binned according to the entanglement-entropy content as discussed in Sec. III A.

The above stochastic process is described by the following classical master equation for the probability of having an entanglement entropy $S$ at time $t$, that we denote $\mathcal{P}_t(S)$:

$$\mathcal{P}_{t+dt}(S) = rdt \int_{\Delta S_{\rm qj}} P(\Delta S_{\rm qj}|S-\Delta S_{\rm qj})\mathcal{P}_t(S-\Delta S_{\rm qj}) + \\ + (1-rdt)\int_{\delta S_{\rm nH}} P(\delta S_{\rm nH}|S-\delta S_{\rm nH}dt) \\ \times \mathcal{P}_t(S-\delta S_{\rm nH}dt) \qquad (19)$$

where the first term describes the jump, which adds a random contribution $\Delta S_{\rm qj}$ with probability $rdt \times P(\Delta S_{\rm qj}|S-\Delta S_{\rm qj})$, with $r$ the resetting rate, while the second one describes the non-Hermitian dynamics, which increase the entanglement of a random slope $\delta S_{\rm nH}$ with probability $(1-rdt) \times P(\delta S_{\rm nH}|S-\delta S_{\rm nH}dt)$.

To understand the role of the first moments of the gain-loss distribution on the entanglement dynamics, it is useful to derive from the master equation [Eq. (19)] a dynamical equation for the average entanglement entropy, $S = \int dS\, S\, \mathcal{P}_t(S)$, which reads

$$\frac{dS}{dt} = \overline{\delta S_{\rm nH}}(S,\ell) + \overline{\Delta S_{\rm qj}}(S,\ell)/\overline{\tau} \equiv \Phi(S,\ell). \qquad (20)$$

This is a straightforward rate equation for the dynamics of the average entanglement entropy $S$, which appear to be controlled by a balance between the average entanglement gain $\overline{\delta S_{\rm nH}}(S,\ell)$ and loss $\overline{\Delta S_{\rm qj}}(S,\ell)$. The fact that these gain-loss rates depend on the value of the entanglement entropy itself, as previously discussed, is crucial here and results in a nontrivial flow of the entanglement entropy with time, encapsulated in the function $\Phi(S,\ell)$ defined in Eq. (20). We emphasize that the key assumption to construct the RW model for the entanglement entropy in Eq. (19), from which Eq. (20) directly follows, is that the rates to move depend on the value of the entanglement entropy itself. While this assumption might seem very fine tuned and it is likely not satisfied in the most

general case, we note that it bares conceptual similarity with certain random-circuit models where analogous phenomenological dynamics for entanglement have been discussed [85–87]. It is an interesting open question, that we leave for future work, to understand whether in certain limiting cases one could derive such an effective stochastic dynamics microscopically. In the present case, this assumption must be verified *a posteriori* with numerical simulations, as we are going to discuss now.

In Fig. 3(b), we plot $\Phi(S,\ell)$ for the Ising chain (at a particular point of the phase diagram). We see that $\Phi(S,\ell)$ vanishes at a value $S = S_\infty(\ell)$, which represents a fixed point of the entanglement stochastic dynamics Eq. (20). This fixed point is attractive, i.e., depending on the initial condition, it is approached either from the low-entangled branch, where $\Phi(S,\ell) > 0$, or from the high-entangled one, where $\Phi(S,\ell) < 0$. According to our simple model, the steady-state entanglement entropy in a monitored system satisfies the equation

$$\Phi(S_\infty,\ell) = \overline{\delta S_{\rm nH}}(S_\infty,\ell) + \overline{\Delta S_{\rm qj}}(S_\infty,\ell)/\bar{\tau} = 0. \quad (21)$$

This relation, which is one of the main results of this work, has a clear and transparent interpretation: the steady-state entanglement entropy in a monitored system is reached when the entanglement gain due to non-Hermitian evolution and the loss due to QJs perfectly balance each other.

We can now benchmark this stochastic model for the entanglement-entropy dynamics. First, in Fig. 3(c), we show that it can reproduce very accurately the dynamics of the average entanglement entropy in the monitored Ising chain, thus capturing the entanglement transition occurring in this model, as we discuss in more detail in Sec. IV. In addition, we can extract the steady-state entanglement $S_\infty$ and its subsystem-size $\ell$ dependence from Eq. (21) and compare them with the full QJ results. As shown in Fig. 3(d), the agreement is really good both at weak monitoring, where it reproduces the logarithmic scaling of the entanglement entropy, and in the area law. We emphasize that the classical stochastic model leading to Eq. (20) is built upon the entanglement gain and loss statistics obtained from the full QJ dynamics. Nevertheless, it still represents a considerable simplification with respect to the full quantum stochastic dynamics. The agreement between the classical model and the full QJ dynamics suggests that only few key features of the many-body state are relevant to describe the stochastic dynamics of the entanglement entropy, irrespective of the microscopic details, pointing toward a sort of universal behavior of quantum jumps and non-Hermitian evolution on entanglement. More importantly, as we will discuss in Sec. IV, it provides a new tool to analyze and decode the scaling of entanglement entropy in monitored systems.

## IV. APPLICATIONS

In this section, we showcase the application of our new metric, the entanglement statistics of gain and loss, to the different models of monitored fermions introduced in Sec. II C and their entanglement dynamics. Unless specified otherwise, throughout this section we consider an initial product state of the form $|\Psi(0)\rangle = |0,1,0,1,\ldots,0,1\rangle$ and open boundary conditions. We fix the hopping along the chains as units of energy and inverse time, $J = 1$. Throughout this work, we consider a system of size $L = 128$ for free fermions and $L = 14$ for the interacting case. We solve the QJ dynamics for noninteracting models using free-fermion techniques (see Appendix F) and the high-order Monte Carlo wave-function method, while for interacting fermions we use exact time propagation with a second-order Trotter expansion.

### A. Monitored Ising chain

We first present our results for the entanglement-entropy dynamics of the Ising chain under QJs, which complete those obtained in Ref. [43,46]. In Fig. 4(a), we present the dynamics of the entanglement entropy for a certain number of stochastic trajectories and compare to the average value and the value obtained in the no-click limit. A first observation is that the no-click limit follows the average entanglement entropy quite closely and the fluctuations appear to remain modest in size.

In Fig. 4(b), we present the scaling of the steady-state entanglement entropy as a function of the subsystem size $\ell$, for different values of the parameters. We see an entanglement transition into an area law as the monitoring rate is increased. The weak-monitoring phase has an entanglement entropy compatible with a logarithmic scaling. Following previous works, we extract an effective central charge $c_{\rm eff}$ by fitting the steady-state entanglement entropy as $S_\ell^\infty = c_{\rm eff} \log \sin \pi \ell/L$. In Figs. 4(c) and 4(d), we plot $c_{\rm eff}$ as a function of $\gamma$ and $h$. We see that increasing either $\gamma$ or $h$ drives a transition into a phase with $c_{\rm eff} = 0$, corresponding to an area-law scaling of the entanglement entropy, in qualitative analogy to the no-click limit (see Appendix A). Still, certain aspects of the phase diagram appear to be different in the QJ case, the most striking one being visible at large field $h > 1$ and small $\gamma$, where the stochastic problem shows a subvolume logarithmic scaling of the entanglement entropy in a region in which, according to the no-click evolution, the system should be in the area law, as already noted in Ref. [46].

We can now use the insight from the stochastic classical model—specifically, the steady-state condition in Eq. (21)—to break down the entanglement-entropy content of the steady state. In particular, in Figs. 4(e) and 4(f) we plot separately the entanglement gain $\overline{\delta S_{\rm nH}}$ and the loss

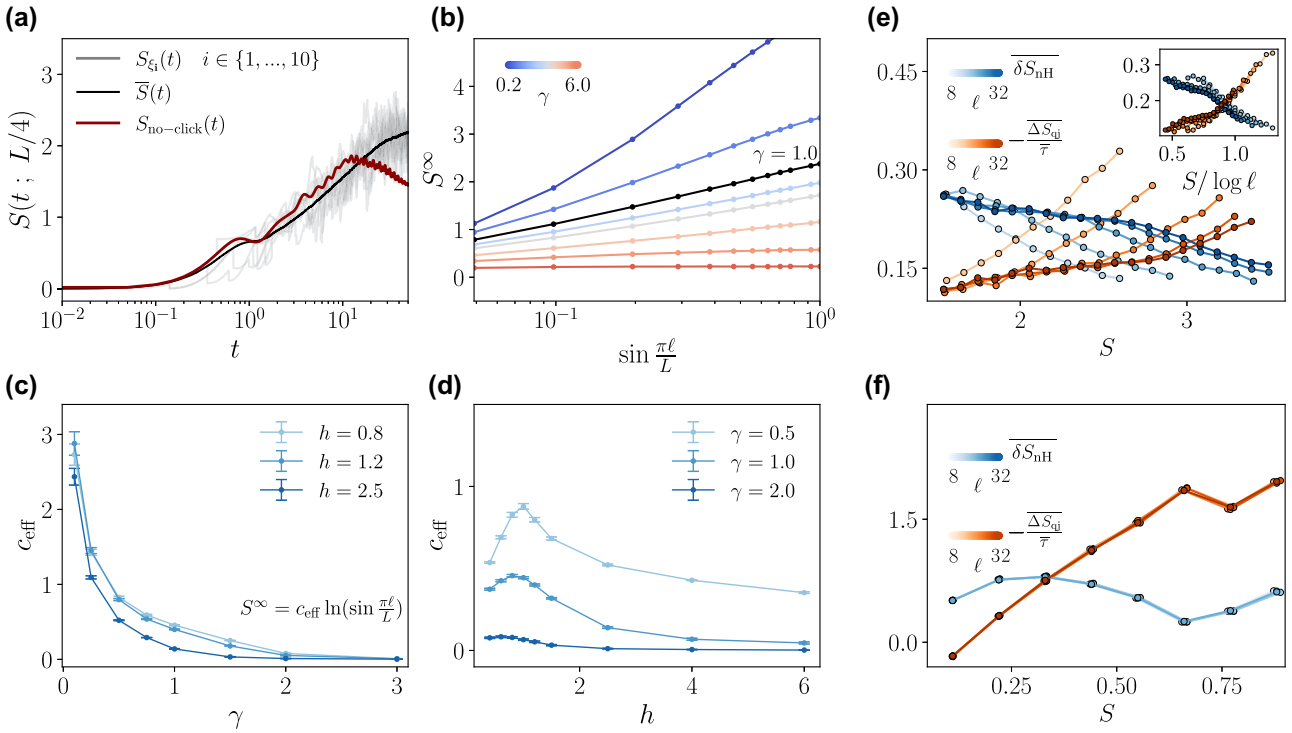


FIG. 4. The entanglement dynamics under QJ monitoring for the Ising chain. (a) A comparison among the average, trajectory, and no-click evolution for measurement rate $\gamma = 1.0$ and $h = 0.4$. (b) The average steady-state entanglement entropy: $\gamma = \{0.2,\ 0.5,\ 1.0,\ 1.5,\ 2.0,\ 3.0,\ 4.0, 6.0]\}$, $h = 0.4$. For weak monitoring, we see a logarithmic scaling that evolves into an area law upon increasing $\gamma$. (c),(d) The phase diagrams as obtained from the effective central charge $c_{\text{eff}}$ as a function of (c) $\gamma$ and (d) $h$. (e),(f) The steady-state entanglement balance: the average entanglement gain $\overline{\delta S_{\text{nH}}}$ and loss $-\overline{\delta S_{\text{qj}}}/\overline{\tau}$, as a function of the average entanglement entropy $S$ and different subsystem sizes $\ell$ (the error bars are smaller than the size of the dots): (e) $\gamma = 0.2$, $h = 0.4$; (f) $\gamma = 3.0$, $h = 0.4$. In the weak-monitoring phase, shown in (e), both contributions scale logarithmically with $\sin \pi \ell / L$ (see the inset), suggesting that the QJs weakly renormalize the non-Hermitian dynamics. Both terms are independent of the subsystem size at strong monitoring (f), leading to an area law.

$-\overline{\Delta S_{\text{qj}}}/\overline{\tau}$ as a function of the entanglement-entropy content $S$ across the phase diagram and for different subsystem sizes $\ell$. According to our classical picture, the steady state is obtained when gain and loss are balanced, corresponding to a value of entanglement entropy at which the two curves match. The scaling with subsystem size of the two contributions tells us about the mechanism driving the entanglement production. In, e.g., the weak-monitoring phase [Fig. 4(e)], both contributions scale logarithmically (see the inset) suggesting that the entanglement gain due to the renormalized non-Hermitian dynamics shows a logarithmic scaling with $\ell$, as in the no-click limit at this value of parameters. Based on these results, we conclude that in the weak-monitoring phase, the non-Hermitian dynamics are only weakly renormalized by QJs. In the area law on the other side [Fig. 4(f)], both gain and loss contributions become essentially independent of the subsystem size, crossing in a low-entanglement region as expected from an area law. A similar analysis can be done in the region of weak-monitoring rate and large field (see Appendix E) and it reveals that again for a moderate field, $h \sim 1$, the non-Hermitian dynamics seem weakly renormalized and drive the logarithmic growth of entanglement entropy, while for large $h$ the non-Hermitian evolution is effectively area law and the contribution due to QJs still has a nontrivial scaling with $\ell$, which is responsible for the observed logarithmic scaling of the entanglement entropy at large values of the field $h$.

### B. Monitored SSH model

We now consider the entanglement dynamics for the monitored SSH model. In Fig. 5(a), we show the evolution of the entanglement entropy for a sample of quantum trajectories for weak monitoring $\gamma = 0.5$, corresponding to the volume-law phase of the no-click limit (see Appendix A). At the level of single-quantum trajectories, it is already evident that QJs have, in this case, a strong impact with respect to the no-click evolution. This is true in particular at weak monitoring, where the no-click dynamics display a linear growth corresponding to the volume-law phase. Here, the stochastic dynamics induced

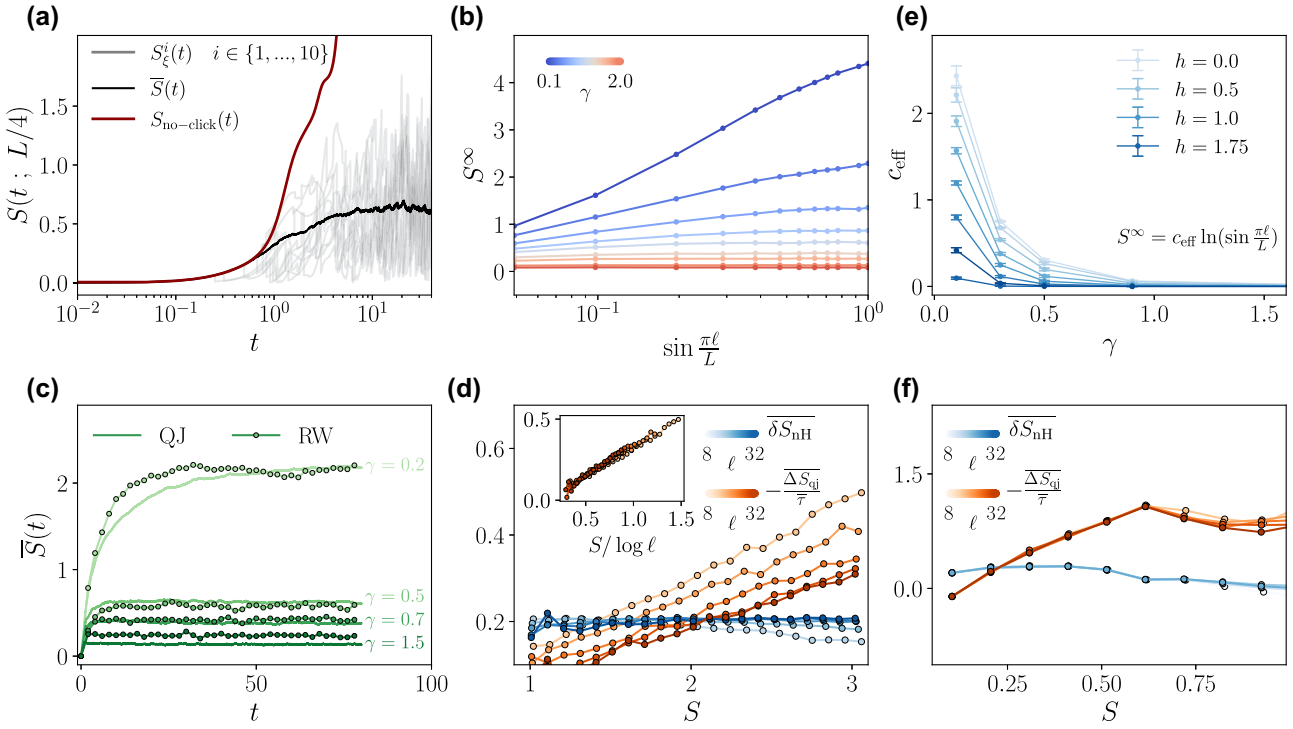


FIG. 5. The entanglement dynamics under QJ monitoring for the SSH chain. (a) A comparison among the average, trajectory, and no-click evolution of the measurement rate $\gamma = 0.5$; $h = 1.0$. (b) The average steady-state entanglement for the monitored SSH model: $\gamma = \{0.1,\ 0.2,\ 0.3,\ 0.4,\ 0.5,\ 0.7,\ 0.9,\ 1.5,\ 2.0\}$, $h = 0.4$. For weak monitoring, we see a logarithmic scaling that evolves into an area law upon increasing $\gamma$. (c) The phase diagram as obtained from the effective central charge $c_{\rm eff}$ as a function of $\gamma$. (d) A comparison between the dynamics of the average entanglement entropy obtained from the exact quantum jump dynamics and the phenomenological classical RW. (e),(f) The steady-state entanglement balance: the average entanglement gain $\overline{\delta S_{\rm nH}}$ and loss $-\overline{\delta S_{\rm qj}}/\overline{\tau}$, as a function of the average entanglement entropy $S$ and different subsystem sizes $\ell$ (the error bars are smaller than the size of the dots): (e) $\gamma = 0.2$, $h = 1.0$; (f) $\gamma = 1.5$, $h = 1.0$. In the weak-monitoring phase, shown in (e), the contributions due to QJs scale logarithmically with $\sin \pi \ell / L$ (see the inset), while the term arising from the non-Hermitian evolution is practically $\ell$ independent. In the strong-monitoring phase, corresponding to the area law, neither contribution depends on $\ell$.

by the quantum jumps effectively suppress the entanglement growth and bring the system to a stationary state that is less entangled than in the no-click limit.

The scaling of the steady-state average entanglement entropy for different subsystem sizes and increasing values $\gamma$ is shown in Fig. 5(b). The entanglement-entropy growth in the weak-monitoring regime is compatible with a logarithmic law, as for the Ising model, from which we can extract an effective central charge $c_{\rm eff}$. As we show in Fig. 5(c), this quantity vanishes as a function of $\gamma$, indicating a transition into an area-law phase. Although affected by the inevitable finite-size effects, our results show that the volume-law phase of the non-Hermitian SSH is not stable when including quantum jumps.

We now show how looking at the statistics of entanglement gain and loss allow us to obtain further insights into the impact of QJs on the monitored SSH. We first show [Fig. 5(d)] that the classical RW model with resetting also perfectly captures the entanglement dynamics for the SSH case. Then, in Figs. 5(e) and 5(f), we look at the steady-state entanglement gain and loss, respectively, for weak and strong monitoring. In the former case, we can see clearly that the jump contribution depends strongly on the subsystem size; the bigger the subsystem, the less QJs decrease the entanglement on average. Interestingly, the subsystem-size dependence of this contribution looks logarithmic, as shown in the inset of Fig. 5(e). On the other hand, the contribution of the non-Hermitian evolution depends weakly on both $\ell$ and $S$, at least for the values of entanglement entropy, which are allowed to be explored by the jumps, i.e., around the crossing point, which corresponds to the steady-state entanglement $S_\infty$. For large monitoring [Fig. 5(f)], on the other hand, we see that both contributions are almost independent of $\ell$ and their crossing occurs in a regime of small entanglement entropy, leading to an area-law scaling.

From this result, we conclude that for the monitored SSH, the logarithmic growth of the entanglement entropy at weak monitoring arises mainly due to QJs. The non-Hermitian dynamics on the other hand, which would lead to a volume law in the no-click limit, are strongly renormalized by the effect of QJs and barely depend

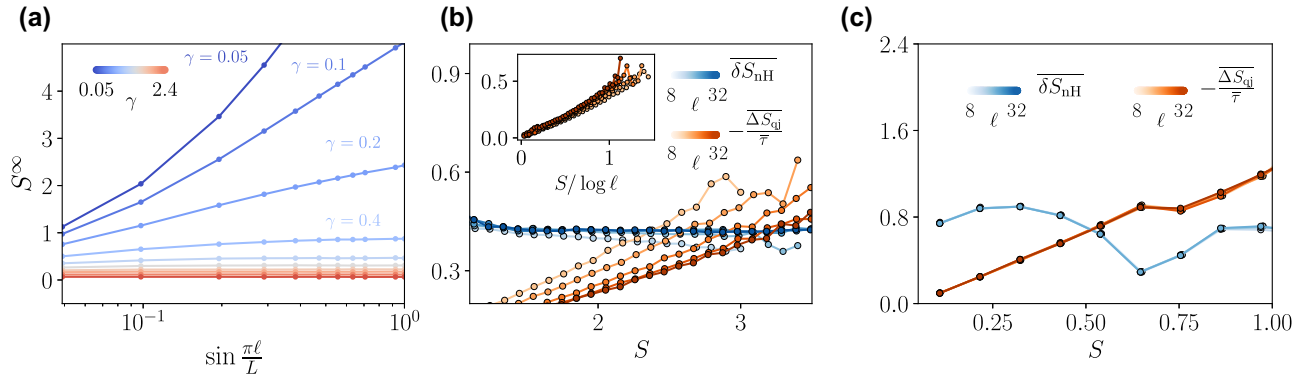


FIG. 6. The entanglement dynamics under QJ monitoring for monitored free fermions with $U(1)$ symmetry. (a) The average steady-state entanglement: $\gamma = \{0.05, 0.1, 0.2, 0.4, 0.6, 0.8, 1.0, 1.2, 1.6, 2.4\}$. For weak monitoring, we see a logarithmic scaling that evolves into an area law upon increasing $\gamma$. (b),(c) The steady-state entanglement balance: the average entanglement gain $\overline{\delta S_{\rm nH}}$ and loss $-\overline{\Delta S_{\rm qj}}/\overline{\tau}$, as a function of the average entanglement entropy $S$ and different subsystem sizes $\ell$ (the error bars are smaller than the size of the dots): (b) $\gamma = 0.2$; (c) $\gamma = 1.0$. In the weak-monitoring phase, shown in (b), the contributions due to QJs scale logarithmically with $\ell$ (see the inset), while the term arising from the non-Hermitian evolution is practically flat. In the strong-monitoring phase, corresponding to the area law, neither contribution depends on $\ell$. The crossing point again corresponds to the zero of $\Phi(S, \ell)$, i.e., to the steady-state entanglement $S_\infty$.

on the subsystem size. In Appendix D, we discuss the dynamics from a highly entangled state to show how, in that case, one could probe the subsystem-size dependence in the non-Hermitian contribution—but only at large values of entropy, far above what the system can explore under the effects of QJs in the dynamics starting from lowly entangled initial states.

### C. Fermions with $U(1)$ symmetry and monitoring of local density

We now present an application of the entanglement gain-loss statistics to the case of monitored free fermions with $U(1)$ symmetry related to charge conservation, a problem that has attracted large interest in the literature. Numerical investigations with different monitoring protocols have reported a transition from a critical phase with logarithmic scaling of entanglement entropy to an area-law phase, for both quantum jumps and the quantum state diffusion (QSD) type of density monitoring [38,39]. The robustness of the weak-monitoring subvolume phase, and hence of the transition, has been questioned in the case of projective measurements, where numerical evidence has supported an area-law steady-state entanglement [31]. This result has been theoretically understood within a replica field-theory calculation [33], which has identified connections with the physics of weak-localization corrections. Given this landscape, it is therefore interesting to discuss what types of insights our analysis based on entanglement loss and gain can provide. To this extent, we first show, in Fig. 6(a), our data for the steady-state entanglement entropy versus the subsystem size, to confirm the presence of a sharp crossover from a logarithmic scaling of the entropy to an area law, consistent with the literature.

We then use our metric of the statistics of entanglement gain and loss to investigate the origin of this log scaling for weak monitoring. Specifically, in Fig. 6(b) and 6(c), we plot the contribution to the steady-state entanglement entropy due to QJs and to the renormalized non-Hermitian evolution. Quite interestingly, we note a behavior very similar to the SSH case, namely, the subvolume (logarithmic, see the inset) scaling of the entanglement entropy is essentially due to QJs, while the non-Hermitian Hamiltonian contribution, renormalized by the jumps, is essentially independent of $\ell$. We therefore see another case in which the no-click limit, which for this problem would describe a purely Hermitian evolution, is strongly perturbed by QJs. For large monitoring, on the other hand, both contributions are independent on $\ell$, which is compatible with the area-law scaling in Fig. 6(a).

### D. Role of interactions

Finally, we conclude this section by discussing the generality of our findings beyond the realm of noninteracting monitored fermions. To this extent, we consider the same model as in the previous section (free fermions with density monitoring) but we include a nearest-neighbor interaction $V \neq 0$ (see Sec. II C). In this case, in the weak-monitoring phase, the entanglement dynamics appear compatible with a volume law. Our interest here is to show whether the entanglement gain-loss picture and the classical stochastic model also continue to work in the case of interacting monitoring systems. In Fig. 7, we show that this is indeed the case. In particular, we plot the histograms of entanglement gain and loss for the interacting model and show that the general features—in particular, the asymmetry of the distributions and the strong peak at zero—also

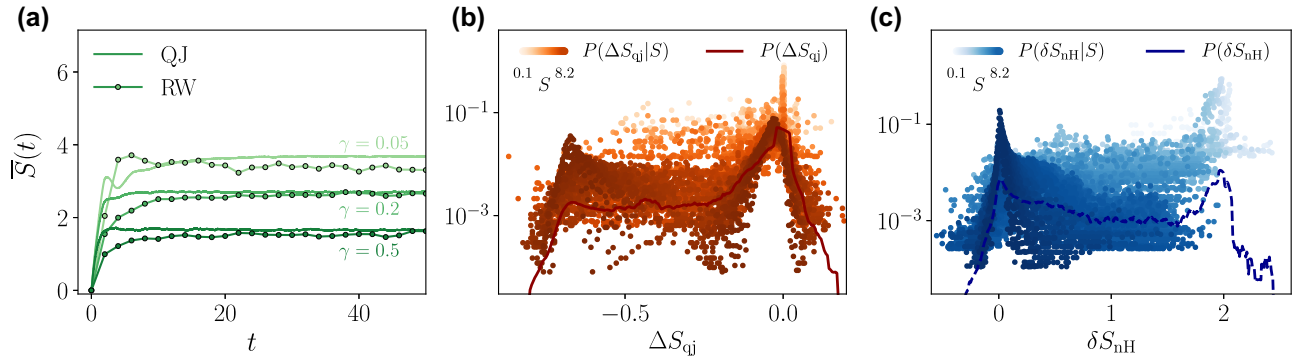


FIG. 7. The entanglement dynamics under QJ monitoring for interacting monitored fermions with $U(1)$ symmetry. (a) A comparison between the dynamics of the average entanglement entropy obtained from the exact quantum jump dynamics and the average of the phenomenological classical RW: 200 classical trajectories are used to perform the average. The steady-state entanglement $S_\infty$ again corresponds to the zero of $\Phi(S,\ell)$ computed from the histograms of (b) and (c). (b),(c) The histogram of the entanglement-entropy change (b) after a QJ $\Delta S_{\rm qj}$ and (c) the one in between QJs $\Delta S_{\rm nH}$, i.e., due to the non-Hermitian evolution.

persist in the interacting case. An intriguing finding is that, as compared to the free-fermionic case, here the role of the entanglement content is somewhat reversed: the probability of having a manifest entanglement change is greater for weakly entangled states than for highly entangled ones. This seems compatible with the expectation that the volume law is stable to the inclusion of measurements: indeed, since entanglement production is particularly important at low entanglement, the loss due to jumps is of lesser significance. On the other hand, having a reduced entanglement loss at large entanglement content should enable the support of a volume-law phase.

## V. DISCUSSION AND IMPLICATIONS FOR FREE FERMIONS MIPT

Our findings for the average entanglement gain and loss have highlighted the concept of renormalized non-Hermitian dynamics. Due to quantum jumps, which effectively reshuffle the initial state onto which the non-Hermitian Hamiltonian act, the effective non-Hermitian dynamics is renormalized with respect to the bare no-click evolution. While for the Ising chain the logarithmic law phase is only weakly renormalized, quantum jumps can strongly impact the dynamics of weakly monitored $U(1)$-conserving models. In particular, in the noninteracting case, quantum jumps completely wash away the no-click volume-law phase. (Nevertheless, the inclusion of non-Gaussian interactions enhances the entanglement growth from the no-click limit, stabilizing a volume-law phase at a low measurement rate.) Our findings therefore highlight a fundamental difference between the weak-monitoring phase of the Ising and the noninteracting $U(1)$ models. While either case, the weak-monitoring phase features a logarithmic scaling of the entanglement entropy, the origin behind this scaling stems from inequivalent mechanisms. In the $U(1)$ symmetric models, the logarithmic scaling comes essentially from the action of the quantum jumps, while for the Ising chain it is the result of the combined effect of jumps and non-Hermitian evolution. This is the same renormalization effect that we have shown to be at play in the monitored Ising chain at intermediate and large field values and can, therefore, naturally explain the departure from the no-click limit.

We conclude with a discussion of the implications of our results for the MIPT of free fermions under quantum jumps. The irrelevance of QJs at weak monitoring in the Ising chain points toward an important role of the non-Hermitian Hamiltonian in this regime. This suggests that the logarithmic phase of entanglement entropy under QJs could possibly be stable in the large system size, as in the no-click case [55]. This is consistent with the replica field-theory prediction for noisy Majorana fermions under QSD [35], although we emphasize the differences in the measurement protocol and unitary dynamics between the two cases. In particular, based on our numerical results, we cannot establish whether in the Ising chain the entanglement scaling is also $\ln^2(\ell)$. On the other hand, our results for the SSH case points toward a strong effect of QJs at weak monitoring. As we have shown, the logarithmic phase found numerically is mainly due to QJs. Their contribution is likely to saturate at large system sizes through a mechanism similar to the weak-localization correction [33].

## VI. CONCLUSIONS

In this work, we have studied the role of quantum jumps on the entanglement-entropy dynamics of monitored quantum many-body systems. A main result is the introduction of a new tool that looks at the statistics of entanglement-entropy gain and loss after or between QJs. We have shown that, quite generically, the resulting histograms display,

particularly for the quantum jump case, a very broad distribution and a typical value pinned close to zero, suggesting that most QJs are not significantly affecting the entanglement entropy controlled by rare jump events. Using the full statistics of entanglement gain and loss, we have built a stochastic RW model with partial resetting, which can reproduce the full QJ dynamics of entanglement entropy. This phenomenological model offers a new light for interpreting the QJ numerics. Indeed, it suggests a natural steady-state condition for the entanglement entropy, given by the balance between gain due to the non-Hermitian evolution and losses due to quantum jumps. Remarkably, this condition accurately reproduces the scaling of entanglement entropy with subsystem size obtained by the full QJ dynamics. Furthermore, it clarifies the origin of the different entanglement scaling and the mutual role of jumps and non-Hermitian evolution.

We have used this framework to decode the mechanism controlling the entanglement dynamics and associated MIPT for three models of monitored free fermions. The outcome of this analysis reveals a compelling difference at weak monitoring between the models with $U(1)$ symmetry, where the renormalized non-Hermitian Hamiltonian does not contribute to the scaling of the entanglement entropy, and the Ising chain, where this renormalization is not present and the no-click limit remains stable to the inclusion of QJs. Finally, we have extended our entanglement gain-loss picture to the case of interacting monitored systems. Remarkably, we have shown that the classical RW model with resetting remains valid and captures the entanglement-entropy dynamics quantitatively. The statistics of entanglement gain and loss for interacting systems suggests that highly entangled states are more robust to quantum jumps—the probability of observing a rare jump that substantially changes the entanglement entropy is smaller for high entanglement content. This is in stark contrast with the case of Gaussian states and can therefore suggests an interpretation for the stability of the volume-law phase at weak monitoring observed in numerical simulations on interacting monitored systems [24].

We envision various follow-ups to this work. First, the presence of an imperfect detector and dissipative interaction with the environment would require adapting the statistics of entanglement gain and loss to entanglement measures valid in open quantum systems, such as the logarithmic negativity or the quantum Fisher information. Another topic of interest for the study of the statistics of entanglement gain and loss is that of higher-dimensional and long-range interacting systems, where nonconformal subextensive phases [47,88] has been identified. Introducing feedback and control would drastically change the phenomenology: these elements will include new source and sink terms in the stochastic model. We leave these generalizations for future work.

## ACKNOWLEDGMENTS

We thank A. Biella, M. Buchhold, J. Dalibard, M. Dalmonte, R. Fazio, A. Paviglianiti, L. Piroli, A. Romito, P. Sierant, and A. Silva for discussions and collaborations on related topics. We acknowledge the computational resources of the Collége de France IPH (Institut de Physique) cluster. X.T. acknowledges the German Research Foundation (Deutsche Forschungsgemeinschaft, DFG) under Germany's Excellence Strategy—Cluster of Excellence Matter and Light for Quantum Computing (ML4Q) EXC 2004/1—Grant No. 390534769 and DFG Collaborative Research Center (CRC) 183 Project No. 277101999—project B01.

*Note added.*—We have recently become aware of a related work studying the stability of the non-Hermitian Hamiltonian for quantum state diffusion [89].

## APPENDIX A: SUMMARY OF ENTANGLEMENT DYNAMICS IN THE NO-CLICK LIMIT

Here, we briefly review the results obtained for the dynamics of the entanglement entropy under purely non-Hermitian evolution driven by $H_{\text{eff}}$, both for the SSH and for the Ising model, corresponding to the no-click limit of the QJ dynamics. In both cases, the time evolution for the entanglement entropy $S_{\text{nH}}(t)$ can be computed exactly in the thermodynamic limit using free-fermion techniques [55,56]. The results have revealed a rich phase diagram as a function of the monitoring strength $\gamma$, which for a non-Hermitian problem is given by the back-action term, and the field $h$ entering the non-Hermitian Hamiltonian. In

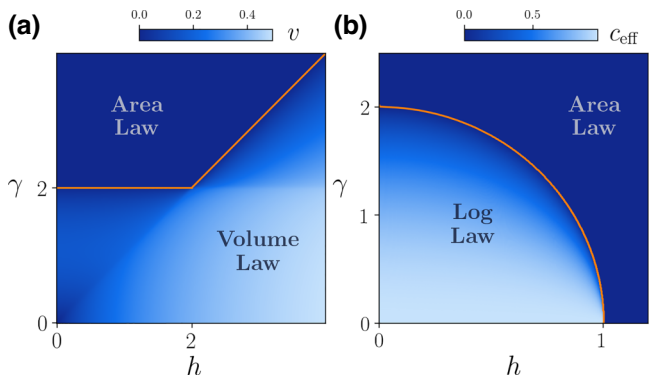


FIG. 8. The entanglement phase diagram of the monitored SSH and Ising models in the no-click limit, corresponding to a deterministic non-Hermitian evolution with $H_{\text{eff}}$. (a) The non-Hermitian SSH and volume-to-area-law transition [56]. (b) The non-Hermitian Ising chain, featuring a transition from a critical phase with logarithmic scaling of the entanglement to an area-law Zeno phase [55]. Note that our convention for the jump operators in Eq. (10) leads to a rescaling of $\gamma$ by a factor $1/2$, with respect to Ref. [55].

Fig. 8, we plot the phase diagram of the two models for completeness.

In the non-Hermitian SSH model in Eq. (14), the weak-monitoring phase for $\gamma < \gamma_c^{\mathrm{SSH}}(h)$, is characterized by an entanglement entropy growing linearly in time, $S_{\mathrm{nH}}(t) \sim t$, and saturating to a stationary value that scales linearly with the subsystem size $\ell$, i.e., $S_{\mathrm{nH}}(t \to \infty) \simeq v\ell$, characteristic of a volume-law phase. This is associated with the purely real spectrum protected by $\mathcal{PT}$ symmetry [56]. The closed-form expression of $v$ allows the complete characterization of the entanglement phases. As the measurement strength $\gamma$ increases at fixed $h$, the prefactor $v$ of the volume-law scaling decreases [cf. Fig. 8(a)] until a critical value is reached when $v = 0$ and the system enters the area-law scaling for the entanglement entropy. This entanglement transition has been shown to be directly related to the spectral transition occurring in $H_{\mathrm{eff}}$ [56]. At weak monitoring, the non-Hermitian quasiparticle spectrum is purely real due to the $\mathcal{PT}$ symmetry of $H_{\mathrm{eff}}$ and as $\gamma$ increases, first the $\mathcal{PT}$ symmetry breaks and some quasiparticle mode acquires a finite lifetime, which induces a sharp decrease of $v$. However, it is only at $\gamma_c^{\mathrm{SSH}}(h)$, when all the quasiparticle modes acquire a finite lifetime, that the system enters the area-law scaling for the entanglement entropy.

In the non-Hermitian Ising chain in a complex transverse field [Eq. (11)], the entanglement entropy has been found for weak monitoring $\gamma < \gamma_c^{\mathrm{Ising}}(h)$ to depend logarithmically on both time and the subsystem size. The corresponding effective central charge $c_{\mathrm{eff}}$, obtained from the ansatz $S_{\mathrm{nH}}(\ell) = c_{\mathrm{eff}} \ln(\ell)$, could be obtained in closed form [55] and has been shown to decrease as a function of both $\gamma$ and $h$ up to the critical line $\gamma_c^{\mathrm{Ising}}(h)$, above which the system has been found to undergo an entanglement transition into an area-law phase [cf. Fig. 8(b)]. As for the SSH case, the entanglement transition for the Ising chains is directly related to a transition in the spectrum of non-Hermitian quasiparticles. The latter separates a critical gapless phase with a vanishing imaginary part of the spectrum at a given point in the Brillouin zone from a gapped phase [52].

## APPENDIX B: STATISTICS OF JUMPS WAITING TIMES

In this appendix, we discuss how QJs are distributed in time, i.e., we compute their WTDs. This quantity has been studied in the early days of quantum jumps, motivated by resonance fluorescence spectra [76,90], and a multitude of applications have been found, from solid-state quantum information [91] to quantum transport [77,92–96] to laser cooling [97]; it is also a key quantity in this work.

In general, computing the WTD is a nontrivial task [77]. There is, however, a special case in which this can be done straightforwardly. Whenever the imaginary part of the non-Hermitian Hamiltonian commutes with the real part (and the initial state is an eigenstate of the non-Hermitian part), then one can conclude that the norm decay is exponential and therefore so is the cumulative WTD, $F = 1 - \exp(-K\tau)$ where $K = \sum_i \langle L_i^\dagger L_i \rangle$. In this case, the time for the next jump can be directly obtained as a function of a random number $r$, as $\tau = -(1/K)\ln r$. Such an instance occurs for a system with local density monitoring and conservation of global particle number [31,38].

Here, this quantity has to be extracted numerically but it emerges naturally from the numerical implementation of stochastic QJ dynamics beyond the first-order Monte Carlo schemes [73]. We start by recalling that the WTD is obtained from the decay of the norm $\mathcal{N}(t) \equiv ||e^{-iH_{\mathrm{eff}}t}|\Psi\rangle||$, which reads in general $\mathcal{N}(t) = \exp(-K(t)t)$, where $K(t)$ represents the back action associated with the non-Hermitian Hamiltonian $H_{\mathrm{eff}}$, i.e., $K(t) = \sum_i \langle L_i^\dagger L_i \rangle$. At short times, the rate of decay of the norm can display fluctuations (depending on the model and the initial state) that can result in biasing of the WTD. However, at sufficiently long times, one expects a Poisson law

$$P_{\mathrm{WT}}(\tau; t \to \infty) \sim e^{-K_\gamma^\infty \tau}, \tag{B1}$$

at least for systems in which the monitoring process is local on each site (where $K_\gamma^\infty$ denotes the steady-state value of $K(t)$, which eventually depends on the monitoring rate $\gamma$).

Our numerical analysis on the monitored Ising and SSH models confirms the expectation that QJs are Poisson distributed. The SSH model displays more pronounced tails in the short-time WTD, caused by fluctuations due to the initial state. Indeed, for the SSH model, the observable $K(t)$ driving the decay of the norm is $K_{\mathrm{SSH}}(t) = 2\gamma \sum_i [n_{A,i}(t) + 1 - n_{B,i}(t)]$, where $n_{A/B,i}(t) = \langle \Psi(t)|c_{A/B,i}^\dagger c_{A/B,i}|\Psi(t)\rangle$. At short times, the observable $K_{\mathrm{SSH}}(t)$ displays significant temporal fluctuations due to the chosen initial condition and the WTD shows longer tails. On the other hand, in the Ising model, jumps try to refill empty sites and keep the total number of particles effectively constant. Thus, $K(t)$ is centered around the average number of particles with small fluctuations. A Poisson distribution of a QJ is typical for systems in which the back-action term is a constant of motion. Interestingly, both models feature the same average waiting time of QJs, as shown in Fig. 9(b), and given by $\tau \sim 1/\gamma L$.

## APPENDIX C: SYSTEM-SIZE SCALING OF ENTANGLEMENT LOSS

In the main text, we have introduced a classical stochastic model for the entanglement-entropy dynamics, which builds upon the entanglement gain and loss statistics. In particular, the role of QJs is to induce an entanglement loss that, in the stationary state, is balanced by the gain provided by the non-Hermitian evolution, as described in

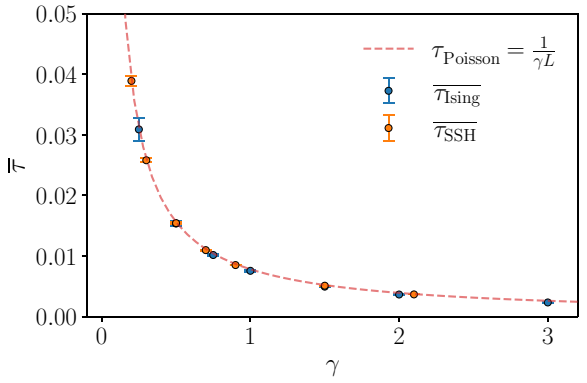


FIG. 9. The average waiting time of quantum jumps in the Ising and SSH models, showing perfect agreement. In both cases, $\overline{\tau} \sim 1/\gamma L$.

Eq. (20). This equation divides the entanglement loss by the average waiting time $\overline{\tau}$, which considers the instantaneous nature of QJs. As we have seen in Appendix B, the average waiting time scales as $1/L$, which raises the question of the stability of the steady-state condition in the large-system-size limit. In this appendix, we provide evidence supporting the statement that the average entanglement loss due to the jump scales as $1/L$, so that the ratio with the averaging waiting time remains finite when $L \to \infty$. In Fig. 10, we plot, for the monitored Ising chain at representative values of the parameters, the average entanglement loss divided by the waiting time, $\overline{\Delta S_{\text{qj}}}(S, \ell)/\overline{\tau}$ as a function of $S$, $\ell$, and different system sizes. We see that the data corresponding to different system sizes collapse onto each other for each subsystem size $\ell$, which demonstrates this invariance of the ratio $\overline{\Delta S_{\text{qj}}}/\overline{\tau}$.

## APPENDIX D: QUANTUM JUMPS FROM HIGHLY ENTANGLED INITIAL STATES

In this appendix, we provide evidence to support the conjecture that highly entangled Gaussian states are more fragile to measurements than weakly entangled ones. To this extent, we consider the monitored SSH chain starting from an initial condition corresponding to the long-time limit of the associated non-Hermitian Hamiltonian, which is known to support volume-law entangled states for small values of $\gamma$ [56]. In Fig. 11(a), we show a sample of trajectories for the entanglement entropy, all converging toward a steady-state value with low entanglement (and equal to the steady state reached from a product state initial condition). In other words, the system under monitoring cannot sustain volume-law entanglement. In Fig. 11(b), we plot the conditional distribution of entanglement loss $P(\Delta S_{\text{qj}}, S)$, which now displays a broadening of its tails, indicating that the role of jumps has become more relevant. In particular, we see that the probability of a large entanglement loss due to jumps at atypical (i.e., high) entanglement content increases, which explains why the initial state entanglement cannot be preserved. In Fig. 11(c), we

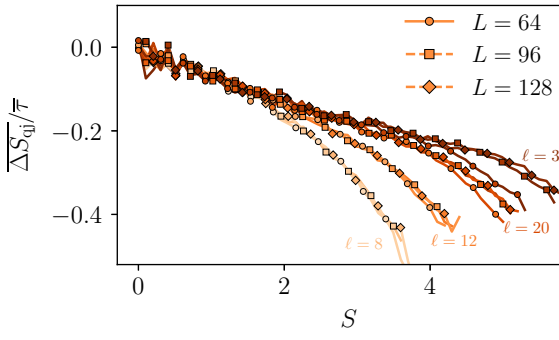


FIG. 10. The loss distribution $\overline{\Delta S_{\text{qj}}}/\overline{\tau}$ obtained in the Ising model for different system sizes $L = 64,\ 96,\ 128$, with $\gamma = 0.2$ and $h = 0.4$. The distribution is invariant regarding the system size; we observe a slight disagreement at large subsystem sizes $\ell$ in the small system $L = 64$, which is due to the finite-size effect.

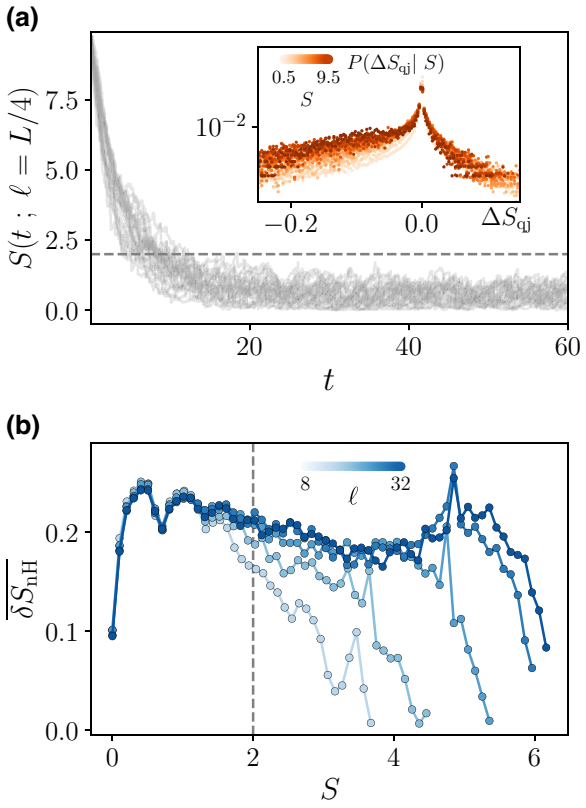


FIG. 11. An analysis of trajectories obtained from a highly entangled initial state in the SSH model. (a) The entanglement dynamics in the monitored SSH chain under QJ dynamics with a highly entangled initial state (namely, a steady state of the no-click limit): $\gamma = 0.2$, $h = 1.0$. In the inset, we show the conditioned version of the distribution $\Delta S_{\text{qj}}$ with respect to the entanglement content when jumps happen. (b) The first moment of the conditioned distribution $\delta S_{\text{nH}}$ as a function of the entanglement content $S$. This quantity is obtained from these trajectories starting from the highly entangled initial state and which allow us to probe the large-entanglement behavior of the distribution.

present the same analysis as given in the main text on the first moment of the gain conditional distribution $\overline{\delta S_{\mathrm{nH}}}$ but for this particular initial condition that allows us to probe entanglement content of higher values. We note that in the region of the steady state (at relatively low entanglement $S \leq 2$ delimited by the dashed line), the average entanglement gain from non-Hermitian dynamics is essentially independent of the subsystem size $\ell$, a behavior similar to what has been observed in Figs. 5(f) and 6(c) for a different initial condition. However, as the system dynamics explore larger values of entanglement entropy ($S \geq 2$), we see important subsystem-size effects in $\overline{\delta S_{\mathrm{nH}}}$. This behavior is usually hidden when starting from a lowly entangled initial condition, because the jumps are confining the dynamics in this lowly entangled space.

## APPENDIX E: MONITORED ISING CHAIN AT LARGE FIELD

In this appendix, we discuss a particular feature of the monitored-Ising-chain phase diagram. Indeed, when considering the region of weak monitoring and large transverse field, deviations from the no-click limit have been reported [40,46]. In particular, here we fix $\gamma = 0.2$ and scan the transverse field for increasing values of $h > 1$, where the no-click evolution predicts an area law for the entanglement entropy but the QJ dynamics still shows a logarithmic scaling. In Figs. 12(a) and 12(b), we repeat our analysis of the average entanglement gain and loss for different subsystem sizes $\ell$. For $h = 1.0$, we again observe a strong $\ell$ dependence in the QJ contribution and the non-Hermitian one. Our steady-state condition [Eq. (21)] predicts a logarithmic scaling for the entanglement entropy, in agreement with the QJ simulation. Moreover, as in the weak-transverse-field limit by breaking down the entanglement content into gain and loss, we note that this log phase is due to a combined effect of the logarithmic scale of both the quantum jumps loss and the renormalized non-Hermitian gain. Upon increasing the transverse field to $h = 4$, we see that the entanglement gain due to the non-Hermitian dynamics becomes essentially $\ell$ independent, in agreement with the no-click limit. On the other hand, the loss due to QJs scales logarithmically with $\ell$ (see the inset), which results in a steady-state entanglement showing a log scaling. As for the weak monitoring of the SSH model, this logarithmic phase is solely due to the QJs.

This analysis therefore highlights two mechanisms at play behind the deviations from the no-click limit observed in the monitored-Ising-chain phase diagram for $h > 1$. At moderate fields, there is a nontrivial renormalization of the non-Hermitian dynamics due to QJs that leads to a log scaling of its average gain contribution, as in the weak-monitoring regime of the model. At larger fields, this renormalization is instead washed away: the non-Hermitian dynamics behaves as in the no-click limit and

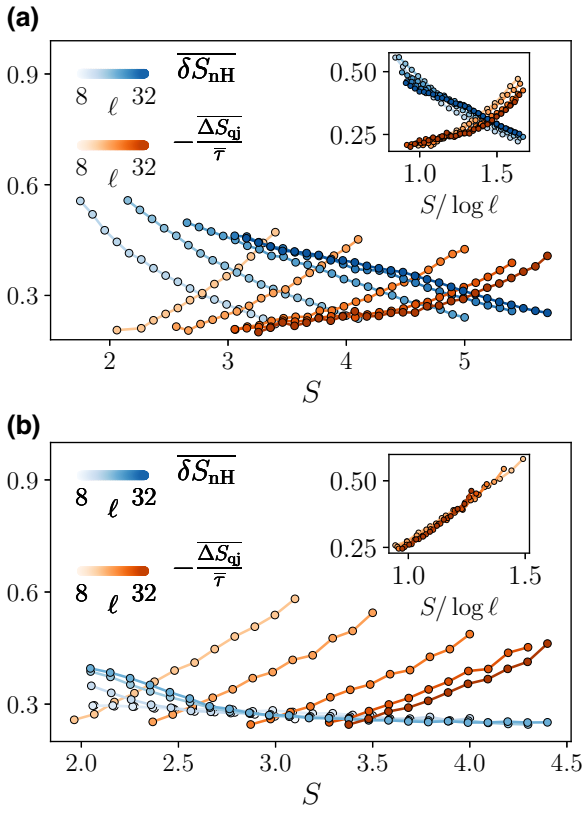


FIG. 12. The steady-state entanglement balance for the monitored Ising chain with large transverse field $h > 1$: the average entanglement gain $\overline{\delta S_{\mathrm{nH}}}$ and loss $\overline{\delta S_{\mathrm{qj}}}/\overline{\tau}$, as a function of the average entanglement entropy $S$ and different subsystem sizes $\ell$. (a) $\gamma = 0.2$, $h = 1.0$; The gain contribution due to the non-Hermitian dynamics acquires a nontrivial $\ell$ dependence that scales logarithmically (see the inset). On the other hand, the QJ loss term also scales logarithmically, which leads to a sub-volume steady-state entanglement absent in the no-click limit. (b) $\gamma = 0.2$, $h = 4.0$; For larger $h$, the non-Hermitian gain term becomes $\ell$ independent, as in the no-click limit. At the same time, the QJ retains a nontrivial scaling (inset), leading to the observed logarithmic scaling.

the logarithmic scaling of the entropy arises only from the jumps. While our numerical results do not allow us to draw conclusions about the large-system-size limit, the above analysis suggests that in the absence of a nontrivial non-Hermitian dynamics, the large-field log phase might eventually saturate at large system sizes into an area law, similarly to the weak-monitoring phase of the SSH model.

## APPENDIX F: FREE FERMION TECHNIQUES WITH QUANTUM JUMPS

This appendix provides details on solving the stochastic Schrödinger dynamics using free-fermion techniques. Since the Hamiltonian that we consider for both models is quadratic and the monitoring process preserves Gaussianity, the state $|\psi\rangle$ is entirely determined by the two-point correlation matrix $C$, due to Wick's theorem.

We can either store the state in this correlation matrix or use another representation based on pure states.

### 1. Correlation matrix

In general, to solve the Schrödinger equation in a free fermions problem, we use Wick's theorem to rewrite the equation in terms of the correlation matrix

$$C(t) = \begin{pmatrix} G(t) & F(t) \\ F(t)^\dagger & 1 - G(t)^T \end{pmatrix}, \tag{F1}$$

where $C_{m,n}(t) = \langle \Psi(t)|\mathbf{c}_m^\dagger \mathbf{c}_n|\Psi(t)\rangle$ is a matrix of size $2L \times 2L$ and $\mathbf{c}^T = (c_1\ c_2\ \cdots\ c_L\ c_1^\dagger\ c_2^\dagger\ \cdots\ c_L^\dagger)$. We obtain, for the deterministic (non-Hermitian) part when measuring the local density, the equation [43]

$$\frac{dC(t)}{dt} = 2i[\mathbb{H}, C(t)] + \gamma C\Lambda C - \gamma \Lambda_+ C\Lambda_+ + \gamma \Lambda_- C\Lambda_-, \tag{F2}$$

where $\Lambda_+ = \mathbb{1}_L \otimes (\sigma_z + 1)/2$, $\Lambda_- = \mathbb{1}_{2L} - \Lambda_+$ and $\Lambda = \mathbb{1}_L \otimes \sigma_z$, $\sigma_z = \mathrm{diag}(1, -1)$ is the Pauli matrix, and $\mathbb{H}$ is defined such that $H = \mathbf{c}^\dagger \mathbb{H} \mathbf{c}$.

The von Neumann entanglement of a subsystem of size $\ell$ can be extracted through the Majorana fermions correlation matrix [43,98]. Effectively, we obtain it by diagonalizing the matrix

$$\mathcal{A}(t) = \begin{pmatrix} \mathcal{G}_\ell^I + \mathcal{F}_\ell^I & \mathcal{G}_\ell^R - \mathcal{F}_\ell^R - \mathbb{1} \\ \mathbb{1} - \mathcal{G}_\ell^R - \mathcal{F}_\ell^R & \mathcal{G}_\ell^I + \mathcal{F}_\ell^I \end{pmatrix}, \tag{F3}$$

with $2G_{\ell\times\ell} = \mathcal{G}_\ell^R + i\mathcal{G}_\ell^I$ and $2F_{\ell\times\ell} = \mathcal{F}_\ell^R + i\mathcal{F}_\ell^I$, which has an imaginary spectrum. The entanglement is given by the formula

$$S_A(t) = -\sum_{j=1}^{\ell} \nu_j(t) \ln\left[\nu_j(t)\right] + (1 - \nu_j(t)) \ln\left[1 - \nu_j(t)\right], \tag{F4}$$

with $\nu_j(t) = (1 - \lambda_j(t))/2$, where the $\lambda_j(t)$ are the $\ell$ eigenvalues of $\mathcal{A}(t)$ with a positive imaginary part.

Jumps such that $L_j \propto n_j$ (i.e., we measure the local density) can be implemented at the level of the correlation matrix. For a jump on site $l$, we have

$$G^J_{m,n} = \begin{cases} 1, & \text{if} \quad n = m = l, \\ 0, & \text{if} \quad m = l, n \neq l \quad \text{or} \quad m \neq l, n = l, \\ G_{m,n} - \frac{G_{m,l}G_{l,n} + F_{m,l}(F^\dagger)_{n,l}}{G_{l,l}}, & \text{otherwise,} \end{cases}$$

$$dF_{m,n} = \frac{G_{n,l}F_{l,m} - G_{m,l}F_{l,n}}{G_{l,l}}. \tag{F5}$$

To avoid numerical instabilities, it is advisable to explicitly write the zeros in the matrix update.

In this work, we implement the sampling of the WTD; therefore, the goal is to find the time at which the jump happens. Thus we need to be able to evaluate the decay of the norm during the non-Hermitian evolution and find the time for the next jump. To do so, we solve numerically the equation

$$\frac{d}{dt}\langle \tilde{\Psi}(t)|\tilde{\Psi}(t)\rangle = -\gamma \langle \tilde{\Psi}(t)|\tilde{\Psi}(t)\rangle \sum_j G_{j,j}(t), \tag{F6}$$

where $G_{j,j}(t)$ is obtained by solving the correlation-matrix equation of motion in parallel and $|\tilde{\Psi}(t)\rangle$ is the unnormalized wave function. Then, for each jump, we can find by bisection the time at which the quantum jump happens [73].

A simplification arises when the model presents a $U(1)$ symmetry because the conservation of the number of particles reduces the size of the correlation matrix that we need to consider by a factor of 2. Indeed, we only have to consider the matrix $G_{m,n}(t) = \langle \psi(t)|\mathbf{c}_m^\dagger \mathbf{c}_n|\psi(t)\rangle$ with $\mathbf{c}^T = (c_1\ c_2\ \cdots\ c_L)$. Here, we give the equation that can be used for the SSH model and, for convenience, we will use a basis respecting the structure of the bipartition $A$ and $B$ of the model; thus we consider the basis in which $c_{2k-1} = c_{A,k}$ and $c_{2k} = c_{B,k}$ for $1 \leq k \leq L/2$. In that case we obtain, for the deterministic part (when measuring $n_{A,i}$ and $1 - n_{B,i}$), the equation [43]

$$\frac{dG(t)}{dt} = 2i[\mathbb{H}, G(t)] + \gamma G\Lambda G - \gamma \Lambda_A C\Lambda_A + \gamma \Lambda_B G\Lambda_B, \tag{F7}$$

where $\Lambda_A = \mathbb{1}_{L/2} \otimes (\sigma_z + 1)/2$, $\Lambda_B = \mathbb{1}_L - \Lambda_A$, and $\Lambda = \mathbb{1}_{L/2} \otimes \sigma_z$ and $\mathbb{H}$ defined such that $H = \mathbf{c}^\dagger \mathbb{H} \mathbf{c}$. Then, the other methods to do the jumps apply directly.

### 2. Wave-function representation

When the system conserves the number of particles, as in the monitored SSH case, not only does the correlation-matrix approach described above simplify but one can also use a different approach based on representing the wave function as

$$|\psi(t)\rangle = P(t) c_{i_1}^\dagger \cdots c_{i_N}^\dagger |0\rangle = \prod_{k=1}^{N} \sum_{m=1}^{L} U_{m,k}(t) c_m^\dagger |0\rangle, \tag{F8}$$

where we consider $N$ particles. Then, the $U(t)$ matrix can be updated through $\tilde{U}(t + dt) = e^{-i\mathbb{H}_{\mathrm{eff}} dt} U(t)$ [29]. Nonetheless, when $H_{\mathrm{eff}}$ is non-Hermitian, the state should be normalized. This is done by performing a QR decomposition on $\tilde{U}(t + dt)$, which normalizes the state without modifying it. The correlation matrix $G(t)$ is then obtained

through

$$G(t) = U(t)^* U(t)^T \qquad \text{with} \qquad \tilde{U}(t) = U(t)R(t). \quad \text{(F9)}$$

We can implement the jumps as previously at the level of this correlation matrix, as in Eq. (F5). In the case of the SSH model, we are also considering jumps of the form $L_j \propto 1 - n_j$ and in that case the update of $G(t)$ is such that

$$G^J_{m,n} = \begin{cases} 0, & \text{if} \quad n = m = l, \\ 0, & \text{if} \quad m = l, n \neq l \quad \text{or} \quad m \neq l, n = l, \\ G_{m,n} + \frac{G_{m,l}G_{l,n}}{1-G_{l,l}}, & \text{otherwise.} \end{cases}$$

The jumps preserve the Gaussianity and $U(1)$ symmetry; thus the new correlation matrix is of the form $G(t) = U(t)^* U(t)^T$ and thus is semidefinite-positive Hermitian, and the $k$th column vector of $U(t)$, called $U_k$, satisfies

$$G(t)U^*_k = U^*_k \qquad 1 \leq k \leq N. \quad \text{(F10)}$$

Then, the SVD decomposition $G(t) = U_{\text{SVD}} D U^\dagger_{\text{SVD}}$ gives these eigenvectors directly and the restriction of the first $N$ columns with eigenvalue 1 (i.e., the $N$ particles) gives

$$U(t) = (U_{\text{SVD}})_{L\times N}. \quad \text{(F11)}$$

Since the columns of $U_{\text{SVD}}$ are orthogonal, the state is well normalized and correctly defined. As in Sec. F 1, we need the decay of the norm to evaluate the time at which the jump is happening. In that case, the norm can be directly obtained from the QR decomposition; indeed,

$$\langle \tilde{\Psi}(t) | \tilde{\Psi}(t) \rangle = \prod_{j=1}^{N} R(t)_{j,j} R(t)^*_{j,j}, \quad \text{(F12)}$$

where $R(t)$ is the matrix from Eq. (F9).

This kind of representation of the wave function can be extended to the general case without particle-number conservation. In that case, we have that [99]

$$|\psi(t)\rangle = \mathcal{N} \exp\left( -\frac{1}{2} \sum_{i,j} \left[ (U(t)^\dagger)^{-1} V(t)^\dagger \right]_{i,j} c^\dagger_i c^\dagger_j \right) |0\rangle, \quad \text{(F13)}$$

where $\mathcal{N}$ enforces the normalization and the evolution is given by imposing that $\gamma_k(t)|\psi(t)\rangle = 0$ with $\gamma_k(t) = \sum_j V^*_{j,k}(t) c^\dagger_j + U^*_{j,k}(t) c_j$. Now, we evolve the two matrices $U(t)$ and $V(t)$ through

$$\begin{pmatrix} U(t) \\ V(t) \end{pmatrix} = e^{-2i\mathbb{H}_{\text{eff}} t} \begin{pmatrix} U(0) \\ V(0) \end{pmatrix}. \quad \text{(F14)}$$

Since the evolution is non-Hermitian, the state here is again not normalized but this can be enforced through the factor $\mathcal{N}$. Importantly, to guarantee that $\gamma_k(t)$ is a well-defined fermionic operator, we have to impose

$$\begin{cases} U(t)^\dagger U(t) + V(t)^\dagger V(t) = \mathbb{1}, \\ V^T(t) U(t) + U^T(t) V(t) = 0. \end{cases} \quad \text{(F15)}$$

This can be done by performing a QR decomposition on

$$\mathbb{U}(t) = \begin{pmatrix} U(t) & V(t)^* \\ V(t) & U(t)^* \end{pmatrix}, \quad \text{(F16)}$$

as proved in Ref. [35]. To implement the jump within this framework, we can compute the correlation matrix $C(t)$, which is given by

$$C(t) = \begin{pmatrix} U(t)U(t)^\dagger & U(t)V^\dagger(t) \\ V(t)U^\dagger(t) & V(t)V^\dagger(t) \end{pmatrix}. \quad \text{(F17)}$$

As in the $U(1)$ case, we then need to retrieve the state matrix, which is done using a SVD decomposition of the correlation matrix.


[1] P. Calabrese and J. Cardy, Evolution of entanglement entropy in one-dimensional systems, J. Stat. Mech.: Theory Exp. **2005**, P04010 (2005).

[2] H. Liu and S. J. Suh, Entanglement tsunami: Universal scaling in holographic thermalization, Phys. Rev. Lett. **112**, 011601 (2014).

[3] A. Nahum, J. Ruhman, S. Vijay, and J. Haah, Quantum entanglement growth under random unitary dynamics, Phys. Rev. X **7**, 031016 (2017).

[4] G. D. Chiara, S. Montangero, P. Calabrese, and R. Fazio, Entanglement entropy dynamics of Heisenberg chains, J. Stat. Mech.: Theory Exp. **2006**, P03001 (2006).

[5] H. Kim and D. A. Huse, Ballistic spreading of entanglement in a diffusive nonintegrable system, Phys. Rev. Lett. **111**, 127205 (2013).

[6] J. H. Bardarson, F. Pollmann, and J. E. Moore, Unbounded growth of entanglement in models of many-body localization, Phys. Rev. Lett. **109**, 017202 (2012).

[7] M. P. Fisher, V. Khemani, A. Nahum, and S. Vijay, Random quantum circuits, Annu. Rev. Condens. Matter Phys. **14**, 335 (2023).

[8] A. C. Potter and R. Vasseur, *Quantum Sciences and Technology* (Springer, Cham, 2022), p. 211.

[9] O. Lunt, J. Richter, and A. Pal, *Quantum Sciences and Technology* (Springer, Cham, 2022), p. 251.

[10] M. J. Gullans and D. A. Huse, Dynamical purification phase transition induced by quantum measurements, Phys. Rev. X **10**, 041020 (2020).

[11] C. Noel, P. Niroula, D. Zhu, A. Risinger, L. Egan, D. Biswas, M. Cetina, A. V. Gorshkov, M. J. Gullans, D. A. Huse, and C. Monroe, Measurement-induced quantum phases realized in a trapped-ion quantum computer, Nat. Phys. **18**, 760 (2022).

[12] J. M. Koh, S.-N. Sun, M. Motta, and A. J. Minnich, Measurement-induced entanglement phase transition on a superconducting quantum processor with mid-circuit readout, Nat. Phys. **19**, 1314 (2023).
[13] Google AI and Collaborators, Measurement-induced entanglement and teleportation on a noisy quantum processor, Nature **622**, 481 (2023).
[14] Y. Li, X. Chen, and M. P. A. Fisher, Quantum Zeno effect and the many-body entanglement transition, Phys. Rev. B **98**, 205136 (2018).
[15] Y. Li, X. Chen, and M. P. A. Fisher, Measurement-driven entanglement transition in hybrid quantum circuits, Phys. Rev. B **100**, 134306 (2019).
[16] B. Skinner, J. Ruhman, and A. Nahum, Measurement-induced phase transitions in the dynamics of entanglement, Phys. Rev. X **9**, 031009 (2019).
[17] M. Szyniszewski, A. Romito, and H. Schomerus, Entanglement transition from variable-strength weak measurements, Phys. Rev. B **100**, 064204 (2019).
[18] C.-M. Jian, Y.-Z. You, R. Vasseur, and A. W. W. Ludwig, Measurement-induced criticality in random quantum circuits, Phys. Rev. B **101**, 104302 (2020).
[19] S. Choi, Y. Bao, X.-L. Qi, and E. Altman, Quantum error correction in scrambling dynamics and measurement-induced phase transition, Phys. Rev. Lett. **125**, 030505 (2020).
[20] A. Zabalo, M. J. Gullans, J. H. Wilson, R. Vasseur, A. W. W. Ludwig, S. Gopalakrishnan, D. A. Huse, and J. H. Pixley, Operator scaling dimensions and multifractality at measurement-induced transitions, Phys. Rev. Lett. **128**, 050602 (2022).
[21] P. Sierant and X. Turkeshi, Universal behavior beyond multifractality of wave functions at measurement-induced phase transitions, Phys. Rev. Lett. **128**, 130605 (2022).
[22] P. Sierant, M. Schirò, M. Lewenstein, and X. Turkeshi, Measurement-induced phase transitions in $(d+1)$-dimensional stabilizer circuits, Phys. Rev. B **106**, 214316 (2022).
[23] K. Klocke and M. Buchhold, Majorana loop models for measurement-only quantum circuits, Phys. Rev. X **13**, 041028 (2023).
[24] Y. Fuji and Y. Ashida, Measurement-induced quantum criticality under continuous monitoring, Phys. Rev. B **102**, 054302 (2020).
[25] O. Lunt and A. Pal, Measurement-induced entanglement transitions in many-body localized systems, Phys. Rev. Res. **2**, 043072 (2020).
[26] E. V. H. Doggen, Y. Gefen, I. V. Gornyi, A. D. Mirlin, and D. G. Polyakov, Generalized quantum measurements with matrix product states: Entanglement phase transition and clusterization, Phys. Rev. Res. **4**, 023146 (2022).
[27] B. Xing, X. Turkeshi, M. Schiró, R. Fazio, and D. Poletti, Phys. Rev. B **109**, L060302 (2024).
[28] A. Altland, M. Buchhold, S. Diehl, and T. Micklitz, Dynamics of measured many-body quantum chaotic systems, Phys. Rev. Res. **4**, L022066 (2022).
[29] X. Cao, A. Tilloy, and A. De Luca, Entanglement in a fermion chain under continuous monitoring, SciPost Phys. **7**, 024 (2019).
[30] L. Fidkowski, J. Haah, and M. B. Hastings, How dynamical quantum memories forget, Quantum **5**, 382 (2021).
[31] M. Coppola, E. Tirrito, D. Karevski, and M. Collura, Growth of entanglement entropy under local projective measurements, Phys. Rev. B **105**, 094303 (2022).
[32] H. Lòio, A. De Luca, J. De Nardis, and X. Turkeshi, Purification timescales in monitored fermions, Phys. Rev. B **108**, L020306 (2023).
[33] I. Poboiko, P. Pöpperl, I. V. Gornyi, and A. D. Mirlin, Theory of free fermions under random projective measurements, Phys. Rev. X **13**, 041046 (2023).
[34] C.-M. Jian, H. Shapourian, B. Bauer, and A. W. W. Ludwig, (2023), arXiv:2302.09094.
[35] M. Fava, L. Piroli, T. Swann, D. Bernard, and A. Nahum, Nonlinear sigma models for monitored dynamics of free fermions, Phys. Rev. X **13**, 041045 (2023).
[36] C. Carisch, A. Romito, and O. Zilberberg, Quantifying measurement-induced quantum-to-classical crossover using an open-system entanglement measure, Phys. Rev. Res. **5**, L042031 (2023).
[37] T. Jin and D. G. Martin, (2023), arXiv:2309.15034.
[38] O. Alberton, M. Buchhold, and S. Diehl, Entanglement transition in a monitored free-fermion chain: From extended criticality to area law, Phys. Rev. Lett. **126**, 170602 (2021).
[39] M. Van Regemortel, Z.-P. Cian, A. Seif, H. Dehghani, and M. Hafezi, Monitoring-induced entanglement entropy and sampling complexity, Phys. Rev. Res. **4**, L032021 (2022).
[40] X. Turkeshi, A. Biella, R. Fazio, M. Dalmonte, and M. Schiró, Measurement-induced entanglement transitions in the quantum Ising chain: From infinite to zero clicks, Phys. Rev. B **103**, 224210 (2021).
[41] T. Botzung, S. Diehl, and M. Müller, Engineered dissipation induced entanglement transition in quantum spin chains: From logarithmic growth to area law, Phys. Rev. B **104**, 184422 (2021).
[42] Y. Bao, S. Choi, and E. Altman, Symmetry enriched phases of quantum circuits, Ann. Phys. **435**, 168618 (2021).
[43] X. Turkeshi, M. Dalmonte, R. Fazio, and M. Schirò, Entanglement transitions from stochastic resetting of non-Hermitian quasiparticles, Phys. Rev. B **105**, L241114 (2022).
[44] G. Piccitto, A. Russomanno, and D. Rossini, Entanglement transitions in the quantum Ising chain: A comparison between different unravelings of the same Lindbladian, Phys. Rev. B **105**, 064305 (2022).
[45] G. Kells, D. Meidan, and A. Romito, Topological transitions in weakly monitored free fermions, SciPost Phys. **14**, 031 (2023).
[46] A. Paviglianiti and A. Silva, Multipartite entanglement in the measurement-induced phase transition of the quantum Ising chain, Phys. Rev. B **108**, 184302 (2023).
[47] T. Müller, S. Diehl, and M. Buchhold, Measurement-induced dark state phase transitions in long-ranged fermion systems, Phys. Rev. Lett. **128**, 010605 (2022).
[48] M. Buchhold, T. Müller, and S. Diehl, (2022), arXiv:2208.10506.
[49] J. Dalibard, Y. Castin, and K. Mølmer, Wave-function approach to dissipative processes in quantum optics, Phys. Rev. Lett. **68**, 580 (1992).

[50] M. B. Plenio and P. L. Knight, The quantum-jump approach to dissipative dynamics in quantum optics, Rev. Mod. Phys. **70**, 101 (1998).

[51] H. M. Wiseman and G. J. Milburn, *Quantum Measurement and Control* (Cambridge University Press, Cambridge, United Kingdom, 2009).

[52] A. Biella and M. Schiró, Many-body quantum zeno effect and measurement-induced subradiance transition, Quantum **5**, 528 (2021).

[53] S. Gopalakrishnan and M. J. Gullans, Entanglement and purification transitions in non-Hermitian quantum mechanics, Phys. Rev. Lett. **126**, 170503 (2021).

[54] S.-K. Jian, Z.-C. Yang, Z. Bi, and X. Chen, Yang-Lee edge singularity triggered entanglement transition, Phys. Rev. B **104**, L161107 (2021).

[55] X. Turkeshi and M. Schiró, Entanglement and correlation spreading in non-Hermitian spin chains, Phys. Rev. B **107**, L020403 (2023).

[56] Y. L. Gal, X. Turkeshi, and M. Schiró, Volume-to-area law entanglement transition in a non-Hermitian free fermionic chain, SciPost Phys. **14**, 138 (2023).

[57] K. Kawabata, T. Numasawa, and S. Ryu, Entanglement phase transition induced by the non-Hermitian skin effect, Phys. Rev. X **13**, 021007 (2023).

[58] T. Orito and K.-I. Imura, Entanglement dynamics in the many-body Hatano-Nelson model, Phys. Rev. B **108**, 214308 (2023).

[59] C. Zerba and A. Silva, Measurement phase transitions in the no-click limit as quantum phase transitions of a non-Hermitean vacuum, SciPost Phys. Core **6**, 051 (2023).

[60] E. Granet, C. Zhang, and H. Dreyer, Volume-law to area-law entanglement transition in a nonunitary periodic Gaussian circuit, Phys. Rev. Lett. **130**, 230401 (2023).

[61] L. Su, A. Clerk, and I. Martin, Dynamics and phases of nonunitary Floquet transverse-field Ising model, Phys. Rev. Res. **6**, 013131 (2024).

[62] T. Banerjee and K. Sengupta, Entanglement transitions in a periodically driven non-Hermitian Ising chain, Phys. Rev. B **109**, 094306 (2024).

[63] G. Lee, T. Jin, Y.-X. Wang, A. McDonald, and A. Clerk, Entanglement phase transition due to reciprocity breaking without measurement or postselection, PRX Quantum **5**, 010313 (2024).

[64] Z. G. Yuto Ashida and M. Ueda, Non-Hermitian physics, Adv. Phys. **69**, 249 (2020).

[65] H.-K. Lau and A. A. Clerk, Fundamental limits and non-reciprocal approaches in non-Hermitian quantum sensing, Nat. Commun. **9**, 4320 (2018).

[66] F. Minganti, A. Miranowicz, R. W. Chhajlany, and F. Nori, Quantum exceptional points of non-Hermitian Hamiltonians and Liouvillians: The effects of quantum jumps, Phys. Rev. A **100**, 062131 (2019).

[67] M. Naghiloo, M. Abbasi, Y. N. Joglekar, and K. W. Murch, Quantum state tomography across the exceptional point in a single dissipative qubit, Nat. Phys. **15**, 1232 (2019).

[68] F. Minganti, A. Miranowicz, R. W. Chhajlany, I. I. Arkhipov, and F. Nori, Hybrid-Liouvillian formalism connecting exceptional points of non-Hermitian Hamiltonians and Liouvillians via postselection of quantum trajectories, Phys. Rev. A **101**, 062112 (2020).

[69] P.-R. Han, F. Wu, X.-J. Huang, H.-Z. Wu, C.-L. Zou, W. Yi, M. Zhang, H. Li, K. Xu, D. Zheng, H. Fan, J. Wen, Z.-B. Yang, and S.-B. Zheng, Exceptional entanglement phenomena: Non-Hermiticity meeting nonclassicality, Phys. Rev. Lett. **131**, 260201 (2023).

[70] C. Ehrhardt and J. Larson, Exploring the impact of fluctuation-induced criticality on non-Hermitian skin effect and quantum sensors (2023), arXiv:2310.18259.

[71] M. Ueda, Nonequilibrium open-system theory for continuous photodetection processes: A probability-density-functional description, Phys. Rev. A **41**, 3875 (1990).

[72] C. W. Gardiner, A. S. Parkins, and P. Zoller, Wave-function quantum stochastic differential equations and quantum-jump simulation methods, Phys. Rev. A **46**, 4363 (1992).

[73] A. J. Daley, Quantum trajectories and open many-body quantum systems, Adv. Phys. **63**, 77 (2014).

[74] H.-P. Breuer and F. Petruccione, *The Theory of Open Quantum Systems* (Oxford University Press, Oxford, United Kingdom, 2002).

[75] M. Radaelli, G. T. Landi, and F. C. Binder, A Gillespie algorithm for efficient simulation of quantum jump trajectories (2023), arXiv:2303.15405.

[76] C. Cohen-Tannoudji and J. Dalibard, Single-atom laser spectroscopy. Looking for dark periods in fluorescence light, Europhys. Lett. **1**, 441 (1986).

[77] G. T. Landi, M. J. Kewming, M. T. Mitchison, and P. P. Potts, Current fluctuations in open quantum systems: Bridging the gap between quantum continuous measurements and full counting statistics, PRX Quantum **5**, 020201 (2024).

[78] H. Carmichael, *Statistical Methods in Quantum Optics 1* (Springer Science & Business Media, Berlin, 1999).

[79] P. Calabrese and J. Cardy, Entanglement entropy and quantum field theory, J. Stat. Mech. **2004**, P06002 (2004).

[80] L. Amico, R. Fazio, A. Osterloh, and V. Vedral, Entanglement in many-body systems, Rev. Mod. Phys. **80**, 517 (2008).

[81] J. M. Hickey, S. Genway, I. Lesanovsky, and J. P. Garrahan, Time-integrated observables as order parameters for full counting statistics transitions in closed quantum systems, Phys. Rev. B **87**, 184303 (2013).

[82] With a slight abuse of notation, we indicate the average over the gain-loss statistics with an overbar, as for the average over trajectories.

[83] M. R. Evans and S. N. Majumdar, Diffusion with stochastic resetting, Phys. Rev. Lett. **106**, 160601 (2011).

[84] M. R. Evans, S. N. Majumdar, and G. Schehr, Stochastic resetting and applications, J. Phys. A: Math. Theor. **53**, 193001 (2020).

[85] C. Jonay, D. A. Huse, and A. Nahum, Coarse-grained dynamics of operator and state entanglement (2018), arXiv:1803.00089.

[86] T. Zhou and A. Nahum, Emergent statistical mechanics of entanglement in random unitary circuits, Phys. Rev. B **99**, 174205 (2019).

[87] X. Feng, B. Skinner, and A. Nahum, Measurement-induced phase transitions on dynamical quantum trees, PRX Quantum **4**, 030333 (2023).

[88] K. Chahine and M. Buchhold, (2023), arXiv:2309.12391.

[89] C. Y. Leung, D. Meidan, and A. Romito, Theory of free fermions dynamics under partial post-selected monitoring (2023), arXiv:2312.14022.
[90] H. J. Carmichael, S. Singh, R. Vyas, and P. R. Rice, Photoelectron waiting times and atomic state reduction in resonance fluorescence, Phys. Rev. A **39**, 1200 (1989).
[91] A. Delteil, W.-b. Gao, P. Fallahi, J. Miguel-Sanchez, and A. Imamoğlu, Observation of quantum jumps of a single quantum dot spin using submicrosecond single-shot optical readout, Phys. Rev. Lett. **112**, 116802 (2014).
[92] T. Brandes, Waiting times and noise in single particle transport, AIP Conf. Proc. **1074**, 102 (2008).
[93] M. Albert, G. Haack, C. Flindt, and M. Büttiker, Electron waiting times in mesoscopic conductors, Phys. Rev. Lett. **108**, 186806 (2012).
[94] G. T. Landi, Waiting time statistics in boundary-driven free fermion chains, Phys. Rev. B **104**, 195408 (2021).
[95] G. T. Landi, (2023), arXiv:2305.07957.
[96] M. Coppola, D. Karevski, and G. T. Landi, Conditional no-jump dynamics of non-interacting quantum chains (2023), arXiv:2311.05515.
[97] F. Bardou, J. P. Bouchaud, O. Emile, A. Aspect, and C. Cohen-Tannoudji, Subrecoil laser cooling and Lévy flights, Phys. Rev. Lett. **72**, 203 (1994).
[98] G. Vidal, J. I. Latorre, E. Rico, and A. Kitaev, Entanglement in quantum critical phenomena, Phys. Rev. Lett. **90**, 227902 (2003).
[99] S. Bravyi, Lagrangian representation for fermionic linear optics, Quantum Info. Comput. **5**, 216 (2005).